Luis Paulo Azevedo Henriques Cunha

The effect of surfactants in the microstructure of silica based aerogels

September 2016

· U C ·

UNIVERSIDADE DE COIMBRA

Cover photo: SEM micrograph of the MTMS-derived aerogel synthesized with 0.75g of CTAB; magnification of 10000x.

Luis Paulo Azevedo Henriques Cunha

The effect of surfactants in the microstructure of silica based aerogels

Thesis Project in the scientific area of Chemical Engineering, supervised by the Professors Luísa Maria Rocha Durães and Pedro Nuno das Neves Lopes Simões and submitted to the Department of Chemical Engineering, Faculty of Science and Technology, University of Coimbra

Supervisors:
Prof. Dr. Luísa Maria Rocha Durães
Prof. Dr. Pedro Nuno das Neves Lopes Simões

Host institutions:
CIEPQPF - Research Centre for Chemical Processes Engineering and Forest Products, Department of Chemical Engineering, Faculty of Sciences and Technology of the University of Coimbra

Coimbra
2016

· U C ·

UNIVERSIDADE DE COIMBRA

"If you're trying to achieve, there will be roadblocks. I've had them; everybody has had them. But obstacles don't have to stop you. If you run into a wall, don't turn around and give up. Figure out how to climb it, go through it, or work around it."

Michael Jordan

Acknowledgments

I'd like to express my deepest gratitude to the following persons:

To my mother and father for providing me with the tools to develop and grow as a person. I will repay you in kind when you become old and gray.

To my little sister for existing and giving me a reason to always be proud.

To my friend and colleague João Vareda for helping me with this work and showing that there are people with good intentions who want to help the others no matter the size of the challenges.

To my friend Isabel Gonçalves, a force to be reckoned with, that always gave me so much.

To the Departamento de Engenharia Mecânica da Universidade de Coimbra for providing the mechanical characterization facilities and to Professor Doctor Amílcar Ramalho for helping me with all the mechanical tests.

To the people in the Departamento de Engenharia Química of Universidade de Coimbra that taught me so much.

To Telma Matias for showing and teaching me how to be better.

To André Ferreira whose expertise with GROMACS and Ubuntu were invaluable and without which I would not have been able to carry out molecular dynamics simulations.

To my supervisor Pedro Simões that guided me through the world of molecular dynamics and taught me always to be cautious with the obtained results.

To my supervisor Luisa Durães without whom I probably would have quitted. I cannot describe into words how much her guidance and help taught me so much.

Thank you.

Abstract

This dissertation aimed to study the effect of three types of surfactants (anionic, cationic and non-ionic) in the properties of silica aerogels synthesized with methyltrimethoxysilane (MTMS). This was accomplished using the sol-gel technology with acid-base catalysis in the synthesis of the gels and adding the surfactants sodium dodecyl sulfate (SDS – anionic), hexadecyltrimethylammonium bromide (CTAB – cationic) or Pluronic F127 (F127 – non-ionic) in the sol stage. Finally, supercritical drying with CO_2 was used to obtain the aerogels.

The chemical, physical and mechanical properties of the synthesized materials were evaluated in order to assess and compare the properties of the various aerogels synthesized with different amounts and types of surfactants.

With the addition of surfactants, it was found that the bulk density of the aerogels decreased ($\rho_{b,\ CTAB} \sim 44$; $\rho_{b,\ SDS} \sim 45$; $\rho_{b,\ F127} \sim 49$ kg.m^{-3}) and gels become more flexible ($E_{0\ to\ 15\%\ strain} \sim 1.2$ kPa). CTAB increases the specific surface area of aerogels while the F127 decreases it ($A_{s,\ CTAB} = 436$, $A_{s,\ F127} = 181$, $A_{s,\ SDS} = 345$ m^2.g^{-1}). It was also observed an apparent increase in the contact angle to about 140° and an average 1% increase in the porosity of the aerogels when compared to the aerogels synthesized without surfactants ($\rho_{b,\ puro} \sim 53$ kg.m^{-3}; $E_{0\ to\ 15\%\ strain} = 4.7$ kPa; $A_{s,\ puro} = 322$ m^2.g^{-1}; $\theta_c = 136°$).

The FTIR and elemental analysis showed the formation of a silica matrix with methyl groups derived from MTMS and also suggested the existence of residual surfactant in the aerogel's structure. On the other hand, the zeta potential (-9.25 mV) determined for aerogel particles suggests that ionic surfactants are those that enable the synthesis of more structured aerogels derived from MTMS, which is also confirmed by the SEM results.

The optimization with success of the type and amount of surfactant to use in the synthesis of these gels was achieved, and some of the properties of the resulting aerogels have improved. Thus, this work helped to understand which are the best surfactants to be used with this precursor and synthesis method for tailoring the material for a given application.

This work also included a preliminary molecular dynamics study applied to the sol-gel system here studied. The performed simulations allowed to conclude that agglomerates of MTMS-derived structures are formed. It was also observed that regardless the number of particles used, a cluster has a maximum of 45 particles at the end of 80 ns and that the presence of surfactant during the formation of clusters appears to reduce the final maximum size of the clusters. Although there are limitations in the computational study, the work here developed gave indications on how, at an atomic-molecular level, the phenomena involved in the aerogel synthesis works. These results, although at an exploratory level, are an advancement to the

state of art, since this type of molecular dynamics studies had not been conducted previously for all the systems in study in this work.

Resumo

Esta dissertação teve como objetivo estudar o efeito de três tipos de surfactante (aniónico, catiónico e não-iónico) nas propriedades de aerogéis de sílica sintetizados com metiltrimetoxisilano (MTMS). Usou-se a tecnologia sol-gel com catálise ácido-base na síntese dos materiais, juntando os surfactantes dodecil sulfato de sódio (SDS – aniónico), brometo de hexadeciltrimetilamónio (CTAB – catiónico) e Pluronic F127, (F127 – não-iónico), recorrendo depois à secagem supercrítica com CO_2 para obter os aerogéis.

Avaliaram-se as propriedades químicas, físicas e mecânicas dos materiais sintetizados de forma a avaliar e comparar os vários aerogéis sintetizados com as diferentes quantidades e tipos de surfactante.

Com a adição de surfactantes concluiu-se que a massa volúmica dos aerogéis diminuiu ($\rho_{b,\ CTAB}$ ~ 44; $\rho_{b,\ SDS}$ ~ 45; $\rho_{b,\ F127}$ ~ 49 kg.m^{-3}) e os géis tornam-se mais flexíveis ($E_{0\ to15\%\ strain}$ ~ 1.2 kPa). O CTAB permite aumentar a área de superfície específica dos aerogéis enquanto que o F127 a faz diminuir ($A_{s,\ CTAB}$ = 436, $A_{s,\ F127}$ = 181, $A_{s,\ SDS}$ = 345 m^2.g^{-1}). Observa-se também um aparente aumento para cerca de 140° de ângulo de contacto e em média 1% na porosidade relativamente aos aerogéis que foram sintetizados sem surfactantes ($\rho_{b,\ puro}$ ~ 53 kg.m^{-3}; $E_{0\ to\ 15\%\ strain}$ = 4.7 kPa; $A_{s,\ puro}$ = 322 m^2.g^{-1}; θ_c = 136°).

O FTIR e a análise elementar revelam a formação de uma matriz de sílica derivada de MTMS e sugerem uma existência residual de surfactante na estrutura do aerogel. Por outro lado, o potencial zeta (= -9.25 mV) determinado para partículas de aerogel indicia que os surfactantes iónicos serão os que permitem sintetizar aerogéis derivados de MTMS mais estruturados, o que também se confirmou através dos resultados de SEM.

Conseguiu-se otimizar com sucesso o tipo e quantidade de surfactante a usar na síntese dos géis, tendo-se melhorado algumas das propriedades dos aerogéis resultantes. Assim, este trabalho contribuiu para se compreender quais os melhores surfactantes a utilizar com este precursor e método de síntese, para o *tailoring* do material para uma dada aplicação.

Esta dissertação também incluiu um estudo preliminar de dinâmica molecular, aplicado ao sistema sol-gel sob análise. As simulações realizadas permitiram concluir que existe a formação de aglomerados de estruturas derivadas de MTMS. Também foi possível verificar que, independentemente do número de partículas usadas, um *cluster* tem no máximo 45 moléculas ao fim de 80 ns, e que a presença do surfactante durante a formação dos *clusters* aparenta reduzir o tamanho máximo final dos clusters. Apesar de existirem limitações no estudo computacional, o trabalho desenvolvido nesse plano deu indicações de como funcionam a nível atómico-molecular os fenómenos envolvidos na síntese do aerogel. Estes

resultados, apesar de resultarem de uma análise exploratória, são um avanço para o estado da arte uma vez que este tipo de estudos de dinâmica molecular nunca tinha sido realizado anteriormente para qualquer os sistemas em estudo no trabalho.

Table of Contents

List of Figures

List of Tables

Acronyms

A	Aerogel
APD	Ambient pressure drying
ASAP	Accelarated surface area and porosimetry
ATB	Automated topology builder and repository
B	MTMS-derived particle SI4
C	MTMS-derived particle SI8
CC	Computational chemistry
CMC	Critical micelle concentration
CTAB	Hexadecyltrimethylammonium bromide
DFT	Density functional theory
F127	Pluronic F127
FF	Force field
FTIR	Fourier transform infrared spectroscopy
GROMACS	Groningen machine for chemical simulations
HTSCD	High temperature supercritical drying
LTSCD	Low temperature supercritical drying
MD	Molecular dynamics
MTES	Methyltriethoxysilane
MTMS	Methyltrimethoxysilane
SCD	Supercritical drying
SDS	Sodium dodecyl sulfate
SEM	Scanning electron microscope
TEOS	Tetraethyl orthosilicate
TMOS	Tetramethyl orthosilicate
VMD	Visual molecular dynamics

Nomenclature

ρ_b	Bulk density	kg.m^{-3}
ρ_s	Skeletal density	kg.m^{-3}
E	Young's modulus	kPa
ε	Strain	-
ϵ	Porosity	%
A_s	Specific surface area	m^2.g^{-1}
θ_c	Contact angle	°
m	Mass	kg
V_b	Bulk volume	m^{-3}
V_{pores}	Pore volume	cm^3.g^{-1}
D	Diameter	m; Å
σ	Stress	kPa
t	time	ns

1 Introduction

1.1 Goals

The aim of this work is, using sol-gel chemistry, to study the effect of different types of surfactants on the microstructure of silica based aerogels derived from trimethoxymethylsilane (MTMS). The chosen surfactants were: Sodium Dodecyl Sulfate (SDS), as anionic surfactant, Hexadecyltrimethylammonium Bromide (CTAB), as cationic, and Pluronic F127 as nonionic surfactant. As the surfactant is added in the beginning of the synthesis, thus before the formation of the sol, the assembly of the silica skeleton is changed, modifying the structural pattern of the network. Therefore, the addition of a surfactant to the chemical system allows the tailoring of the aerogel properties without changing its composition, since the surfactant is removed during supercritical drying. The addition of different types and amounts of surfactants allows, via characterization, to find the synthesis conditions that most improves the desired properties of a MTMS-derived aerogel.

The end purpose of the present work is to synthesize lightweight, extremely flexible monolithic aerogels that may also show good insulation performance, in order to be used in spatial and/or terrestrial applications. Improvements in the materials properties are expected to be from a more regular silica network.

In order to compare the synthesized aerogels, characterization techniques such as bulk density determination, helium picnometry, contact angle, Fourier Transformed Infrared Spectroscopy (FTIR), elemental analysis, zeta potential, Accelerated Surface Area and Porosimetry (ASAP), high-resolution scanning electron microscopy (HR-SEM) and uniaxial compression tests were employed.

This work also includes a preliminary molecular dynamics based study on the chosen sol-gel systems, performed with the GROMACS package. Molecular modeling and simulation has recently emerged as an attractive tool to establish connections between experimental and theoretical work in the chemical engineering field. In spite of being limited by the available computational resources, these simulations provide relevant insights, at a molecular level, into the changes that might occur in the studied sol-gel systems due to the presence of the surfactants.

1.2 Motivations

In recent years, researchers have found aerogels to be good candidates in several applications including space environments, building construction, decontamination of polluted media, etc. Silica aerogels are the most studied aerogels because their chemistry is easy to control. However, silica aerogels are fragile and moisture sensitive, which are their major drawbacks. The use of organically modified silica precursors, like MTMS, solves the problem of degradation by water and brittleness, as the incorporated methyl groups make the aerogel super hydrophobic and flexible. Still, there is a lack of regularity in the obtained structural pattern that may be solved in order to improve the aerogels properties.

The requirements for materials to be used in space environments are very tight, which means that further improvement of already good characteristics, such as low thermal conductivity and density, and high specific surface area of silica aerogels, is required. As such, the motivation for this work is to contribute to enhance these characteristics so that aerogels can have wider use in both aerospace technology and building construction, their most studied applications.

There is a shortage of information in literature on the effect of different types of surfactants in silica based aerogels. This work aims at shedding a light to the best type of surfactant to use in order to achieve a set of desired characteristics for an aerogel. Surfactants were chosen as additives to the synthesis as it is recognized that they can induce more regularity in the structuring of the silica matrix, giving controlled pore size and reducing the predominance of macropores in the monolith when compared to mesopores.

The effects of additives in sol-gel chemistry are usually evaluated in terms of final macroscopic properties that the material exhibits, but these are caused by changes in the materials microstructure. HR-SEM analysis and ASAP can give an insight into the obtained microstructure. However, these techniques do not allow us to understand the occurred changes at a molecular level, and we do not know precisely what kind of interactions happen or how the system truly behaves during gelation. The molecular dynamics simulations of the system under study comes from the need to have a better understanding of what might really occur in the structuring of the gel at a molecular level.

1.3 Thesis Structure

This dissertation is divided in 5 chapters that show the work developed during the semester.

Chapter 2 approaches the fundamentals of silica-based aerogels, their properties and applications and the surfactants used. The fundamentals behind molecular dynamics and the

computational tools employed are also described. The state of the art surveying the use of surfactants in the synthesis of MTMS-derived aerogels and the study of cluster conformation for these aerogels is also presented.

Chapter 3 presents the experimental and computational procedures used throughout this thesis. The methods for characterizing both the synthesized materials and analyzing the computational results are discussed here.

Chapter 4 exhibits the results obtained and their discussion.

Chapter 5 has the concluding remarks and the future prospects.

2 Fundamentals

This chapter presents the basic theoretical framework behind the study developed in this thesis in a way that the reader may find it easier to understand. Concepts related with aerogels, sol-gel processes, surfactants, computational chemistry and molecular dynamics are summarized in this chapter.

2.1   Aerogels – Historical Note and Silica Based Aerogels

The term aerogel was firstly used by Samuel Stephens Kistler, in 1932[1], to designate gels in which the liquid phase was replaced by a gas, without collapsing the continuous solid network and, as such, having minimal shrinkage of the gel. To do this, Kistler applied a new drying technique that allowed the removal of the liquid that impregnated the gels after being transformed into a supercritical fluid; this was called supercritical drying. It was carried out in an autoclave, increasing the pressure and temperature so that they would exceed the critical pressure and temperature of the liquid entrapped in the gel pores. With this drying method, Kistler prevented the formation liquid-vapor menisci at the exit of the gel pores, which develop tension between the liquid and the pore walls and results in capillary pressure gradients and, thus, shrinkage of the gel[1].

After the definition proposed by Kistler, a new designation was needed for the gels that had significant shrinkage of the solid network due to evaporative drying. The chosen name was xerogels. In this regard, IUPAC's definition for xerogels seems to be too wide because it defines xerogels as an "Open network formed by the removal of all swelling agents from the gel"[1].

Initially, aerogels were essentially made from metal salt precursors that could give origin to an oxide gel [1]. Nowadays, silica is one of the most common materials from which aerogels are composed. Silica based aerogels have a nanostructured silica backbone and usually have high specific surface area, high porosity, low density, low dielectric constant and excellent heat and acoustic insulation properties [2].

2.2   Properties and Applications of Silica Based Aerogels

Silica aerogels are amorphous ceramic materials, made from siloxane ($\equiv$Si–O–Si$\equiv$) bonds, and they can be composed by either hydrophobic or hydrophilic matrices. They can also show

hard/brittle or soft/flexible behavior and these features are mainly dependent on the precursor used. The precursors can be mono, di, tri or tetrafunctional, depending on the RO/Si ratio. With increasing R- substitution for R–O–Si≡, more ≡Si–O–Si≡ bonds are formed [1]. Some examples of these precursors and their effect in the properties of the aerogels are shown in Table 2.1. The one studied in this thesis is Methyltrimethoxysilane.

Table 2.1 - Examples of precursors for silica aerogel synthesis (adapted from [3]).

Hydrophilic precursors	Hydrophobic precursors
Tetramethyl orthosilicate (TMOS)	Methyltrimethoxysilane (MTMS)
Tetraethyl orthosilicate (TEOS)	Methyltriethoxysilane (MTES)
Hard and brittle aerogels	Soft and flexible aerogels

With different precursors, it is possible to tailor the final properties of the silica based aerogels within an already pre-established range of desired values. Table 2.2 summarizes some of the typical properties of silica aerogels.

Table 2.2 - Typical properties of silica aerogels and MTMS aerogels. (adapted from [1][3][4])

Property	Aerogels (orthosilicates)	Aerogels (MTMS)
Bulk density	$0.1 - 0.35$ g.cm^{-3}	$0.040 - 0.1$ g.cm^{-3} [5][6][7]
Skeletal density	~2 g.cm^{-3}	~1.2 g.cm^{-3} [5][6]
Porosity	$80 - 95\%$	>94% [5][6][7]
Specific surface area	$500 - 1000$ m^2.g^{-1}	$232 - 411$ m^2.g^{-1} [5][6]
Average pore diameter	$20 - 40$ nm	3.4 nm [5]
Primary particle diameter	$2 - 5$ nm	-
Dielectric constant	~1.1	-
Thermal conductivity	0.015 W.m^{-1}.K^{-1}	0.037 W.m^{-1}.K^{-1} [7]

This unique set of properties, despite the fact that these materials are not yet completely ready for large-scale fabrication, urged the research and development of these materials for well-defined niche markets, even at higher manufacturing costs. Table 2.3 sums up some of the possible applications for aerogels [1].

Table 2.3 - Possible applications for aerogels regarding their properties [3].

Property	Features	Applications
Thermal conductivity	Good thermal insulation; Withstands high temperature; Light weight	Building construction and appliance insulation; Automobiles, space vehicles
Density/porosity	Lightest synthetic solid; High surface area	Sensor; Storage device; Adsorbents; Catalysts supports; Templates
Optical	Transparent; Low refractive index	Light guides; Cherenkov detectors
Acoustic	Low speed of sound; Good sound insulation	Sound proof rooms
Mechanical	Elastic; Lightweight	Energy absorber; Hypervelocity particle trapping
Electrical	Low dielectric constant; High dielectric strength; High surface area	Dielectrics for integrated circuits; Capacitors; Spacers for vacuum electrodes

With the standard values of properties and the applications of silica based aerogels already defined, an explanation on their manufacturing process is given in the following section.

2.3   Sol-gel Technology

The materials studied in this thesis are obtained by sol-gel technology. This method allows the synthesis of nanostructured materials, in particular metal/metalloid oxides. The process starts with a mixture of precursors dispersed in solution and consists in the transition from a colloid solution of primary particles (dispersed phase is smaller than 1000 nm), i.e. a "sol" [3][8], to a gel, in which the solid particles are arranged in a three-dimensional solid network structure that entraps the solvent [3][9]. This method of processing can be done with metal or metalloid precursors such as salts, alkoxides, oxides, hydroxides, complexes, amines and acrylates as long as they are soluble in the chosen solvent to create materials with uniform, small particle size and varied morphologies [3].

Some of the reasons to choose the sol-gel technology to create ceramic materials are summarized in Table 2.4.

Table 2.4 - Characteristics of sol-gel processing [3][10].

Sol-gel processing
• Process that forms a ceramic material from a liquid at room temperature
• Precise control over the purity of the material
• Bottom-up approach: manipulation of the materials at molecular scale
• Yields the highest specific surface area of the methods for processing ceramics
• Flexible process: it can specifically create composites with considerably different properties that are otherwise not possible.
• Can combine organic and inorganic materials.

All methods of aerogel production by sol-gel technology encompass three major steps: gel preparation, aging of the gel and the drying of the gel (Figure 2.1).
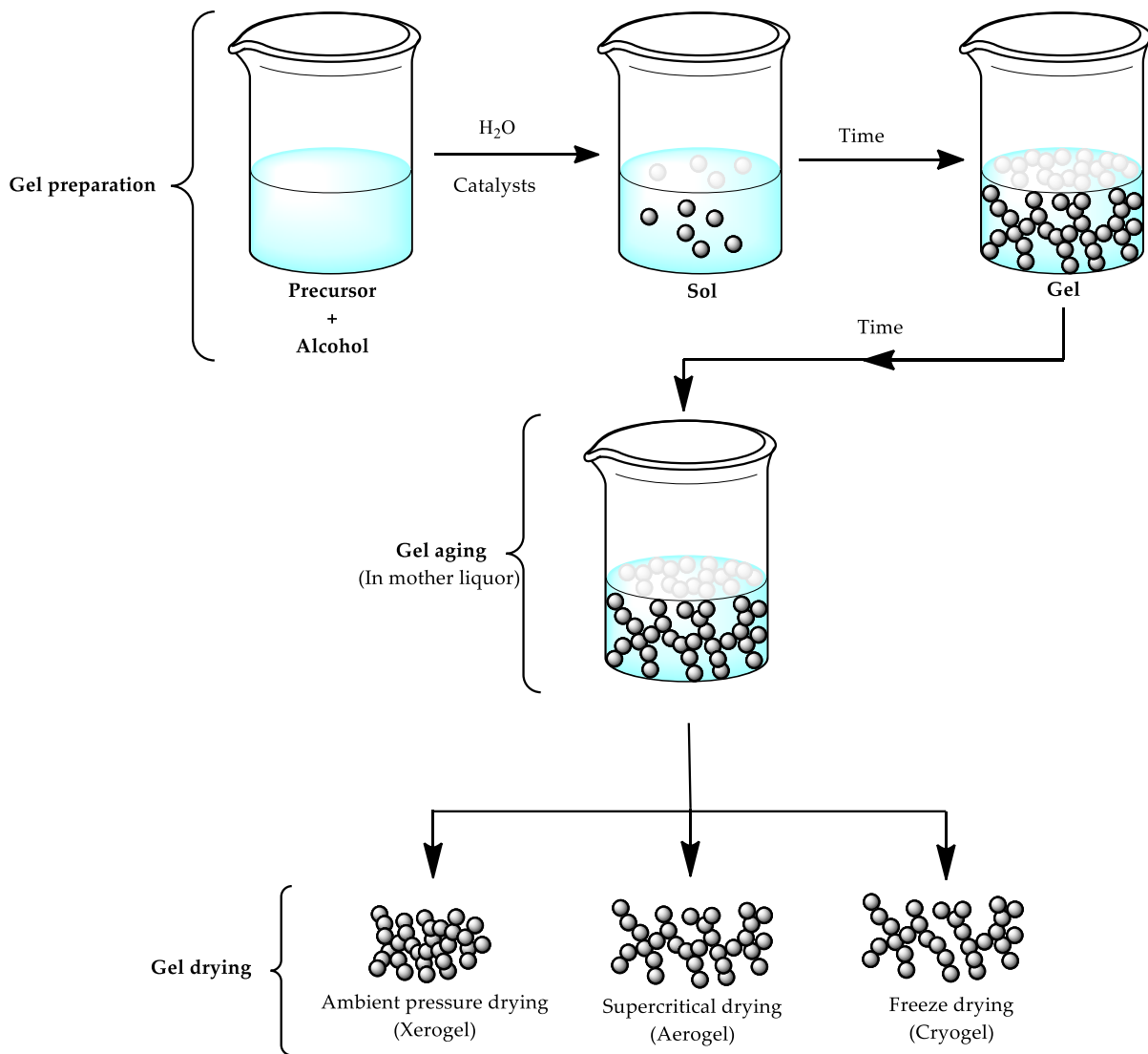
Figure 2.1 - Schematic representation of typical sol-gel synthesis.

2.3.1 Gel preparation

In the gel preparation stage, the precursors are mixed and the hydrolysis and condensation reactions occur. It is necessary to access the reactivity of the desired precursors in order to ensure that these are reactive enough to form a gel. The selected precursors are mixed in a liquid medium in which they are soluble/miscible. Small size alcohols are often used as solvents (ex. methanol, ethanol) for alkoxide precursors. This is due to the fact that silicon alkoxides have low solubility/miscibility in water and are miscible in several organic solvents [2][3][11]. The reactional medium also contains a certain amount of water equivalents that are needed for the hydrolysis of the precursors, the first step of the gel preparation.

Hydrolysis

The hydrolysis reaction occurs between the precursor and water molecules, resulting in hydrolyzed species and an alcohol (in the case of alkoxides). Equation 2.1 exemplifies the hydrolysis chemical reaction for a generic silane alkoxide precursor [1].

$$\equiv Si(OR) + H_2O \ \rightleftharpoons \ \equiv Si(OH) + R(OH) \tag{2.1}$$

The amount of water present in the system influences the extent of the precursors hydrolysis. Thus, it is necessary to add enough water equivalents to have a complete hydrolysis. As the water added to the mixture can be easily manipulated, it acts as a system parameter.

Condensation and gelation

The condensation reactions occur when the previously hydrolyzed species react with one another, creating siloxane bonds ($\equiv Si - O - Si \equiv$) and releasing water molecules, as shown in Equation 2.2 for a generic silane precursor [1].

$$\equiv Si(OH) + (OH)Si \equiv \ \rightleftharpoons \ \equiv Si - O - Si \equiv + H_2O \tag{2.2}$$
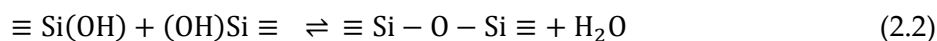
It may also be possible to have a chemical reaction between a hydrolyzed and a non-hydrolyzed precursor species, which instead of producing a water molecule, forms an alcohol one. It is at this stage that the primary particles are formed, building the sol [3].

Since these reactions are carried out at room temperature, their kinetics are slow and, thus, may require several days to reach completion. Therefore, catalysts are used to speed up the sol-gel reactions. With the acid condition the hydrolysis reaction is favored, while with an alkaline condition a higher condensation rate is possible. Thus, a complete control over the gelation process is achieved by separating these conditions through the addition of acid and basic catalysts [3][4], whose effects are shown in Table 2.5. Using a two-step acid-base catalysis is often required and generates similar results to those achieved with basic catalysis [3].

Table 2.5 - Effects of the catalyst on the sol-gel chemistry of silica gels ([2][3][11]).

pH < 6 (acid catalyst)	pH > 8 (base catalyst)
Hydrolysis is favored	Condensation is favored
Linear chains	Branched chains
Low crosslinking	High crosslinking

These reactions are reversible, which means that the gel formed can revert back to a sol state if the conditions at which the gel is formed are changed. This behavior is more common with acid catalysis, in which the silica chains can easily redisperse in solution [3]. With control over the gelation process it is possible to reduce the gelation time but also and more importantly control the nanostructure of the gel. Other parameters that affect the nanostructuration of the resulting gel are the nature of the solvent, the molar ratio between

precursor and water, the molar ratio between precursor and solvent, and the type of surfactants and their molar ratio relatively to the precursor, which are the targets of this study [1][3].

Gelation is identified when there is an abrupt increase in the sol viscosity and a process similar to polymerization, which is called polycondensation, occurs. At this stage, the hydrolysis and condensation reactions are considered complete. Polycondensation occurs in all directions, forming a 3D matrix that occupies the entire volume of the sol, entrapping the solvent. Figure 2.2 exemplifies this matrix for a trialkoxysilane precursor. Particles start to aggregate with one another, going from primary to secondary particles, and form crosslinked chains in a pearl-necklace like matrix [2][3].
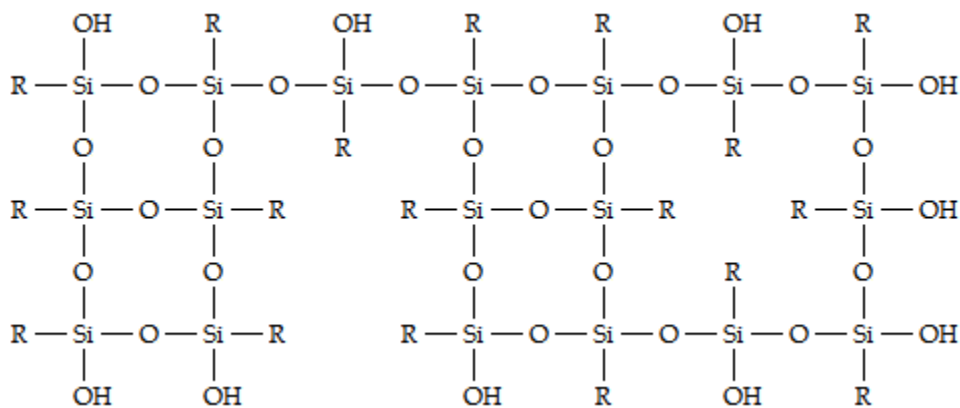
Figure 2.2 - Example of a solid network from a gel formed with a tri-functional silane alkoxide.

2.3.2 Aging of the gel

Gel aging is carried out to strengthen the gel network in order to sustain the tensions the material will be subjected to in the drying step. With the gel being reinforced, shrinkage and the presence of cracks will be minimized, allowing the control of the macroscopic properties of the gel. The reinforcement of the network takes place through the thickening of the necks between secondary particles and Ostwald ripening [1][4]. This happens due to further condensation with residual silanols and, also, because dissolution/reprecipitation of silica occurs as the reactions of hydrolysis and condensation are reversible.

Ostwald ripening is basically the dissolution/reprecipitation of small particles and the filling of small pores, thus giving origin to bigger particles. On the other hand, the neck thickening happens by mass diffusion throughout the liquid and silica precipitates in these "necks" between particles [1][4][12]. During the aging, expulsion of liquid from the network also happens due to the slight contraction induced by the strengthening, in a phenomenon known as syneresis.

Aging may occur either in the liquid solution from the previous step or in a specifically prepared solution. Therefore, it is possible to control and optimize this step by paying attention to parameters like the composition of the liquid phase and its pH, the temperature and pressure.

2.3.3   Drying of the Gel

Depending on the type of gel drying, 3 different types of materials can be produced: xerogels, aerogels and cryogels. With xerogels being the ones that are dried at ambient pressure, aerogels those dried at supercritical conditions and cryogels the ones originated by freeze drying [2].

To make xerogels, the pressure is atmospheric and the temperature is raised in order to evaporate the liquid phase (Ambient Pressure Drying – APD). This drying method leads to the development of capillary stresses in the gel matrix, with large pressure gradients that causes mechanical damage and collapse of the pores as the liquid evaporates from the pores. The collapse is due to the presence of hydroxyl groups that are brought together through capillary forces and, because these are easily reactive groups, they react with one another forming more siloxane bridges and thus irreversibly shrinking the network. As such, xerogels have high tendency to shrink, becoming denser and developing cracks [2][3][4].

This drying technique, although being much more inexpensive when compared to the next two that are going to be described next, has these problems of severe shrinking of the gel and its densification. In order to create aerogel-like materials through ambient pressure drying, other strategies were investigated to overcome these drawbacks. These are focused on the minimization of capillary forces and reduction of liquid-solid interactions. The modification of the silica surface with hydrophobic groups or the use of solvents with low surface energy, or even the use of drying control additives, such as surfactants, can significantly influence the drying process [2].

As said in section 2.1, Kistler was the first that implemented a plan to completely avoid the shrinkage and collapse of the gel by using a supercritical drying approach [1]. Drying with supercritical fluids can be done either at high temperatures or using supercritical CO_2 and drying at low temperatures, but their principle is basically the same. It is aimed to eliminate the capillary forces due to the vapor-liquid equilibrium by surrounding the equilibrium line and surpassing the critical point to achieve the supercritical state region [4].

In high temperature supercritical drying (HTSCD), the gel is put together with a sufficient amount of solvent in an autoclave and the temperature and pressure are raised and adjusted to reach supercritical conditions of the solvent (usually the critical temperature if above 240°C and the critical pressure is above 60 bar). These conditions, when set, are kept

constant for a certain amount of time and then the supercritical fluid is slowly vented out at constant temperature, until atmospheric pressure is reached. At this point, the autoclave is let to cool down to room temperature. The use of organic solvents in high temperature supercritical drying leads to rearrangements in the structure of the gel. For example, the reesterification of the surface of silica based aerogels may occur [4].

In low temperature supercritical drying (LTSCD), the gel is put in an autoclave and then supercritical CO_2 is pumped into the sealed vessel dissolving the organic solvent and extracting it from the gel. When the supercritical state of CO_2 is reached, the outlet valve is opened and CO_2 is continuously pumped for some time to ensure it drags and dissolves all the solvent. This drying approach has practically no impact on the gel's structure and also allows the preparation of hybrid aerogels, since their organic component does not degrade at low temperatures [4]. Table 2.6 shows characteristics of both high and low temperature supercritical drying.

Table 2.6 - Main differences between high and low temperature supercritical drying [4][13].

	HTSCD	LTSCD
Temperature	>240°C	40°C is enough for CO_2 ($T_{sc}\approx31$°C)
Pressure	> 50 atm	< 80 bar (CO_2 $P_{sc}\approx73$ atm)
Additional solvent	No additional solvent required	CO_2 is required
Nanostructure changes	Rearrangements happen	No impact
Use of organic components in precursors	No (they degrade at the used temperatures)	Possible to create hybrid materials

In freeze drying, the solvent is frozen and then sublimed under vacuum. This process forms crystals within the nanostructure that lead to cracked or even powder-like silica products. Water in the solid state has a greater volume than in the liquid state, thus big crystals are formed during freezing. In order to mitigate this, solvents with low expansion coefficients and high sublimation pressure (provided that the used equipment reaches their freezing point) can be used, as well as liquid nitrogen because it freezes the solvent fast enough to form only small crystals [2][4].

2.4   Surfactants

Surfactants touch our everyday lives in countless ways. Being present in our food, drinks, cleaning products, *etc.,* we have been taking them for granted due to their immense potential and versatility in several areas. Since the start of their use in the past century (besides soap), the use of surfactants has matured and evolved to newer possibilities such as the ones presented in the next two subtopics. Their use in gel's synthesis is common, as they aid in the structuration of the solid network.

2.4.1   Surfactants Characteristics

Surface active agents, or simply surfactants, are organic compounds with at least one lyophilic and one lyophobic group. The lyophilic group (polar or ionic) has affinity for polar solvents while the lyophobic group (non-polar) has affinity to non-polar liquids. Surfactants are molecules with at least one non-polar group and one polar (or ionic) group [14]. Figure 2.3 presents a typical representation of a surfactant with a lyophilic "head" and a lyophobic "tail".
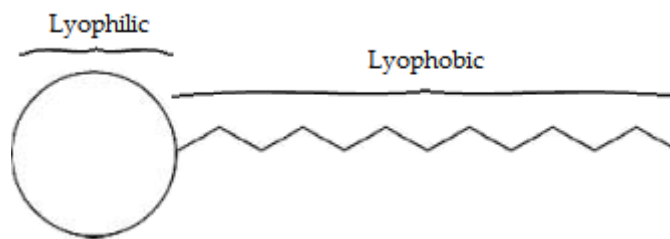
Figure 2.3 - Typical representation of a surfactant.

Due to the opposing forces within a surfactant molecule two phenomena are possible, adsorption and aggregation. The adsorption process occurs when surfactant molecules position themselves in the interface between two immiscible liquids, in order to minimize the contact between the lyophobic and lyophilic phases, resulting in changes in the properties at the interface [14].

Another way to minimize the contact is by aggregation of the surfactant molecules and form what are called micelles. These micelles form even at very low concentrations, at a point that is called critical micelle concentration (CMC) [14]. Various possible micelle types are shown in Figure 2.4.
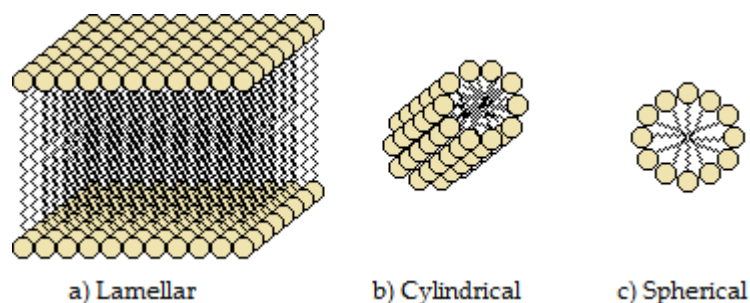
Figure 2.4 - Typical micelle configurations.

These micelles are interesting because they create domains within the solution where particular solutes can be solubilized or emulsified; one good example of micelles is the membrane of cells, in biology, where these domains are vital for the cells activity [14].

A surfactant may carry a negative or positive charge, both or no charge at all. Thus, they can be classified as anionic, cationic, amphoteric (or zwitterionic), behaving at the same time as anionic and cationic surfactants at some pH levels) or non-ionic, respectively [14].

Some applications of surfactants are shown in Table 2.7 to illustrate their diversity.

Table 2.7 - List of some applications of surfactants (adapted from Farn (2006) [14]).

Area of application	Example
• Agrochemical formulations	Water dispersible granules
• Civil engineering	Bitumen additives to give wet adhesion to road aggregates
• Cosmetics and toiletries	Shampoos, soap, bubble baths and shower gels
• Detergents	Dishwashing liquids; Clothes washing liquids/powders
• Food industry	Food grade emulsifiers

2.4.2 Surfactants and MTMS Based Aerogels - State of the Art

Surfactants applied in sol-gel technology are mainly used as templates, acting as porogenic agents by occupying space in the forming matrix of the gel, and also as structure-directing agents (SDAs). Since surfactants tend to organize themselves, it is also theoretically possible to tailor the gel nanostructure to create mostly mesopores (2 – 50 nm). This is a cooperative assembly process between organic surfactants and inorganic precursors (or hybrid precursors, like the MTMS used in this thesis) that form inorganic/organic mesostructured composites. Hence, the surfactant self-assembly is an essential part for the formation of ordered mesostructures [15]. In this way, the resulting gel-matrix which will have an ordered network with the lowest interface energy due to the adsorption phenomenon of the surfactants in the precursors molecules [15].

Table 2.8 and Table 2.9 present the works elected as support for this thesis. These are connected with this thesis, because they used at least one surfactant and the MTMS precursor.

Table 2.8 - Articles from literature with experimental procedures of interest for the present work, presenting gel synthesis with MTMS and surfactants.

Article	Chemical System	Experimental Procedure	Relevant Conclusions
Hayase *et al.*, 2013[16]	**Precursor/Co-precursor:** MTMS and DMDMS **Solvent:** Methanol **Catalysts:** Acetic acid and urea **Surfactant:** n-hexadecyltrimethylammonium chloride (CTAC)	•Stirred for 60 min. to promote hydrolysis; •Solution placed in an oven for gelation at 80°C for several hours; •Washing with alcohol; •Drying at APD conditions.	•Copolymerization with different alkoxysilanes improves the chemical properties of the gels; •Introduction of different functional groups leads to superhydrophobic materials for use as a compound separation medium; •Elastic properties (80 % recovery ratio) are maintained over a wide range of temperature.
Hayase *et al.*, 2012[17]	**Precursor:** MTMS **Solvent:** Methanol and 2-propanol **Catalysts:** Acetic acid and urea **Surfactant:** CTAC	•One-pot sol-gel process; •The starting composition includes 10 mL of aqueous acetic acid (5 mM), 0.40 g of CTAC and 3 g of urea dissolved in a glass sample tube; •5 mL of MTMS are added to the solution under stirring for 30 min at room temperature; •Gelation and aging at 60°C, in a closed vessel, for 4 days; •For 8 hours, the gel is washed with methanol and 2-propanol, three times each; •Supercritical drying with CO_2, for 10 h., at 80°C and 14 MPa; •Molar ratios used: MTMS:water:acetic acid:urea:CTAC $1:1.6 \times 10:1.4 \times 10^{-3}:1.4:3.6 \times 10^{-2}$.	•Transparent aerogels; •Different surfactant/precursor molar ratios change the light transmittance: (0.10 g of CTAC [CTAC]/[MTMS]=0.009 to 0.40 g of CTAC [CTAC]/[MTMS]=0.036); •The light transmittance decreases with increasing quantity of CTAC; •Concentrations of catalysts affect the network and porous structure of the gels; with more urea the lower aerogel density is obtained; •An increasing ratio of solvent/MTMS leads to higher shrinkage; •Using the surfactant, the minimal density of 0.045 g.cm^{-3} is obtained. •Property values: $\rho_b > 45$ km.m^{-3}, T < 91 %, $\epsilon \geq 90$ %, E > 0.8 MPa

Table 2.8 - Articles from literature with experimental procedures of interest for the present work, presenting gel synthesis with MTMS and surfactants. (Cont.)

Article	Chemical System	Experimental Procedure	Relevant Conclusions
Kanamori et al., 2009[18] and Kanamori et al., 2011 (1)[19]	**Precursor:** MTMS **Solvent:** Methanol and 2-propanol **Catalysts:** Acetic acid and urea **Surfactant:** CTAC; CTAB and Pluronic F127	• Two-step sol-gel process; • Two types of systems tested: one with CTAB/CTAC (1 mM) and the other with F127 (5 mM); • The process starts with 20 mL of aqueous acetic acid, stirred at room temperature, for 30min, with either 0.80 g of CTAB/CTAC or 2.0 g of F127, 6.0 g of urea and 9.51 g of MTMS; • Gelation and aging at 60°C, in a closed vessel, for 3 days; • For more than 8 h., the gel is washed with methanol and 2-propanol, three times each; • Supercritical drying with CO_2, for 10 h., at 80°C and 14 MPa; • Molar ratios used: MTMS:water:acetic acid:urea 1:15.9:0.0172 (1mM) or 0.0860 (5 mM):1.43.	• Gels obtained with CTAB or CTAC consists of aggregated particles, while gels obtained with F127 consists of continuous fibrous networks; • More transparent gels, smaller pores and more regular porous structures in aerogels occurs with CTAB or CTAC; • SAXS measurements suggest that the aerogels consist of particle aggregates, and suggest the presence of micropores; • Nitrogen adsorption confirms the presence of micropores, with more micropores for systems containing F127; • Compressive mechanical properties (E = 0.98 MPa for CTAB, 0.87 for CTAC and 0.95 for F127. Recovery of 74, 78 and 75 % respectively for CTAB, CTAC and F127) are related with particles diameter in CTAB and CTAC systems.
Kurahashi et al., 2012[20] and Kanamori et al., 2011 (2)[21]	**Precursor:** MTMS **Solvent:** Methanol **Catalysts:** Acetic acid and urea **Surfactant:** F127; F108; F68; P105; L35; P123	• One-pot process; • Solution of 10 mL or 6 mL of aqueous acetic acid (5 mM), 0-1 g of surfactant and 0.5-3 g of urea are stirred till the solution reaches homogeneity; • 5 mL of MTMS are added and the solution is stirred, at room temperature, for 30 minutes; • Gelation occurs at 60°C during 4 to 5 days; • The gel is washed for 8 hours at 60°C; • Solvent exchange with 2-propanol at 60°C; • Supercritical drying with CO_2 at 80°C and 14 MPa for 10hours or APD at 40°C during 5 days.	• The molecular weight and the PO/EO ratio[1] influence the suppression of the phase separation; • Surfactants with high molecular weight, F127, suppress the phase separation; • In the article of Kurahashi, the aerogels are opaque for surfactants with very high or very low molecular weights; • When using F127 macro and mesopores are formed, depending on its concentration; • The structure is defined by the amount of solvent - with smaller amounts of solvent, the structures become thinner and with less volume.

[1] PO/EO ratio stands for the ratio between Poly(propylene oxide) and Poly(ethylene oxide) in the surfactant molecules.

Table 2.9 - Articles from literature with experimental procedures of interest for the present work, presenting gel synthesis with MTMS.

Article	Chemical System	Experimental Procedure	Relevant Conclusions
Rao *et al.*, 2006[22] and Rao *et al.*, 2005[23]	**Precursor:** MTMS **Solvent:** Methanol **Catalysts:** Oxalic acid ($C_2H_2O_4$) and ammonium hydroxide (NH_4OH)	•Two-step acid-base process; •Solution with acidic water (bidistilled water and 0.001 M of oxalic acid); •Mixing methanol, MTMS and the acid solution; •Stir for 30 minutes; •After 24 h, (10 M) NH_4OH is added to the solution drop by drop; •Gelation at 27°C and aging for 2 days also at 27°C; •Supercritical drying at 265°C and 10 MPa; •One-pot process was also tried where all the components are added at the same time and left stirring for 10 minutes at room temperature.	•Obtained aerogels are highly flexible (up to 60% strain under compression) and hydrophobic to a molar ratio of MTMS:methanol:water of 1:35:8 and remain thermally stable at 530 K; •Young's Modulus decreases to 0.03 MPa with the decrease in density of the materials to 40 kg.m^{-3}; •Very high contact angles (164-173°); •Size of the structural units has a dominant role in the roughness of the surface; •Uniform structural units are obtained for a molar ratio of MTMS:methanol:H_2O:NH_4OH of 1:35:4:3.5x10^{-1}.
Durães *et al.*, 2012[6]	**Precursor:** MTMS **Solvent:** Methanol **Catalysts:** Oxalic acid ($C_2H_2O_4$) and ammonium hydroxide (NH_4OH)	•Two-step acid-base process; •Acid and basic catalysts solutions previously prepared: 0.01 M oxalic acid solution and 10 M ammonium hydroxide solution; •The precursor is mixed with the solvent and the oxalic acid solution at 25°C; •After 24 h, NH_4OH is slowly added at 25°C; •Gelation occurs in an oven at 27°C followed by aging for 2 days; •The gels are dried either by APD, giving xerogels, or by SCD, giving aerogels; •Molar ratios used: MTMS:solvent:acidic water:basic water 1:35:4:4	•The drying method and conditions do not appear to have an influence on the chemical/composition of the obtained materials; •The drying influences the bulk density; •With SCD the lowest density (53.4 kg.m^{-3}) and highest porosity (> 95%) is attained; •The best aerogels are obtained with low heating rates (80°C/h); •APD can be tuned to obtain xerogels with properties similar to aerogels.

From the presented works, only the research group of Kanamori *et al.*, (2009 [18], 2011(1) [19], 2011(2) [21]) and Kurahashi *et al.*, (2012) [20] tested the effect of several surfactants on the structure and properties of MTMS-derived aerogels. However, the synthesis system was different, delivering rigid aerogels. These works used different catalysts (acetic acid and urea) from the ones used in this work. In the current work, the synthesis of gels was done via a two-step acid-base process with oxalic acid and ammonium hydroxide catalysts, similar to the systems presented in Rao *et al.*, (2005) [23], Rao *et al.*, (2006) [22] and Durães *et al.*, (2012) [6], which gives flexible, ultra-lightweight aerogels.

Some of the surfactants used in this work were also used in works of Table 2.8, such as the CTAB and Pluronic F127. However, there was no report until now where the surfactant SDS was tested in similar synthesis conditions. Moreover, one main goal of this work was to elaborate a comparative study (using the same synthesis method) between three major types of surfactants, a cationic (CTAB), an anionic (SDS) and a nonionic (Pluronic F127), and shed light onto the different interactions these can have with the silica species during gelation. In this way, it will be possible to define which type of surfactants will be preferred to tailor the structure and properties of the MTMS-derived aerogels. Such a study was never performed up to our knowledge.

2.5   Computational work

This thesis includes a molecular dynamics study on the interactions between the silica gel's structural units and surfactants. It was then essential to define what was needed to model the formation of a silica gel, the surfactant molecules and the conformations to be used. In the studied system, the gel system is composed by the solvent methanol, the precursor MTMS and a cationic or anionic surfactant (CTAB and SDS respectively) and, as such, their force fields (see below) were required.

Some assumptions are needed for the modeling of such system, namely:
- the temperature and pressure of the simulation;
- the pH level (changed by the addition of OH^- or H^+);
- only the precursor forms clusters;
- the type of structures created in the beginning of condensation of the precursor;
- the force fields to be used;
- simulation time.

To make clear this part of the work, a brief explanation on the meaning of computational chemistry, molecular modeling/simulation and molecular dynamics will be given below.

Computational chemistry and molecular modeling

Broadly speaking, computational chemistry (CC) is the field of chemistry that uses mathematical models and computational methods for the calculation of molecular properties and/or molecular behavior [24]. Nowadays, many research studies are being done in order to simulate and predict how certain systems evolve. This approach allows to minimize the waste of material and human resources doing experimental work, making CC the fastest, cheapest and the best way to test and explore more options in the developing of new molecules [24].

CC simulations can be done by several different more or less demanding methods, like *ab initio*, density functional theory (DFT) and semi-empirical, but the simplest and least time consuming are those based on molecular mechanics (MM). MM avoids the remarkable

complexity of quantum mechanics methods and algorithms thereof. It uses a much simpler mathematical and computing framework, thus allowing to model and simulate the behavior of even extremely large molecules, like proteins, because less computational resources are required.

Before explaining the basic theory behind MM, the concept of energy used therein, which is one of the most important concepts in CC, is presented. The energy of a molecular system is dependent on its kinetic and potential energies that derive from the vibrational, rotational, translational, electronical and nuclear energies and also by the Coulomb law [24]. The total energy of the system is represented by the Hamiltonian operator.

All the methods in CC define the most stable system as the one that has the lowest energy level. Thus, when analyzing the system's energy, the ability of a molecular process to occur can be anticipated [24].

When using MM, the total energy of the molecules in study is given by a simple algebraic equation holding constants obtained by either spectroscopy data or *ab initio* calculations. The set of these equations with their corresponding constants or parameters is called a force field (FF), whose performance is dependent on several factors, namely [24]:

- the functional form of the energy expression;
- the data used to parameterize the FF;
- the technique used to optimize constants from that data;
- the ability of the user to apply the technique in a way consistent with its strengths and weaknesses.

The FF equations describe various aspects of the molecule, such as: bond stretching and bending, torsions, electrostatic interactions, van der Waals forces and hydrogen bonding [24].

Most of the energies used in MM are conformational energies, which means that the computed energies try to reliably predict the energy differences between different conformations. It should also be noted that each conformation has a FF and due to the existence of many FF developed by third parties, researchers rarely have the need to parameterize FF, meaning that existing ones can be used [24].

Molecular dynamics

Molecular dynamics (MD) is a computer simulation method in which atoms and molecules are treated as moving particles, under the influence of classical mechanic FF. This method, firstly developed in the 1950s, is a powerful tool in engineering and science and is used to understand the behavior of fluids and materials at the atomistic level. With MD, it is also possible to directly evaluate physical properties of interest. Regarding chemical engineering applications, several simulations can be made, namely [25]:

- organic mixtures;
- diffusion in nanoporous materials;

- molten salts and room temperature ionic liquids;

- physical properties (FF, vapor pressure and vapor-liquid equilibria, liquid density, self-diffusivity, viscosity, polymer properties such as glass transition temperature and gas penetrant permeation).

Force fields in molecular dynamics

MD treats atoms as classical particles. Since the Hamiltonian of the system only depends on the position and momentum of the collection of atoms, the energetic interactions between atoms are well modeled using FF [25], i.e. the potential energy of the molecular system is described in a FF. MD uses empirical FF that are only dependent on the position of atoms. These empirical FF are approximations because the parameters are obtained experimentally or by *ab initio* calculations.

As all simulations are done with the defined parameters in the FF, the results must be cautiously analyzed because, if the FF are poorly described, the results will not yield practical significance. In this case, the FF will have to be recalculated.

MD solves the Newton equations of motion for a system with N atomic interactions by describing the potential energy of the system. That is done by summing various atomic contributions such as: the bonding interactions, including bond stretching, angular variations and bond twisting, and the nonbonding terms, such as the electrostatic and the van der Waals interactions. Thus it is utmost important to have these parameters well defined because they compose the FF of a molecule that is then used in the molecular dynamics of a system.

Boundary conditions

The simulation is done within a simulation box. However, this box does not have boundaries to prevent boundary effects. This "box without boundaries" is achieved by using the concept of periodic boundary conditions which consists in an array of identical copies, in all directions, of the simulation box. With this concept, every time a particle leaves the box with a set momentum another identical appears on the opposite side of the box, thus preserving the mass, number of particles and the total energy in the simulation box. This model makes an accurate approximation to an infinite box [26].

2.5.1 GROMACS

GROMACS stands for GROningen MAchine for Chemical Simulations and was designed in the University of Groningen, Netherlands, as a package to perform molecular dynamic simulations and energy minimizations [27]. It was primarily designed for molecules that have complicated bond interactions, such as proteins, lipids and nucleic acids, but due to GROMACS ability to calculate the nonbonded interactions extremely fast, it is also possible to use it for research on non-biological systems like the one presented in this thesis [28].

In this thesis, GROMACS is used as a computational tool, for which some basic knowledge is required in order to use it effectively. Since the used FF were obtained from the Automated Topology Builder (ATB) and Repository [29], a treatment before the calculations is required so that the FF from ATB can be computed by GROMACS. Following the treatment, the simulation box is built and then an energy minimization is carried out, at the desired temperature and pressure, to relax the system before performing the trajectory calculations. Figure 2.5 presents a typical flowchart illustrating the different steps used in this thesis.
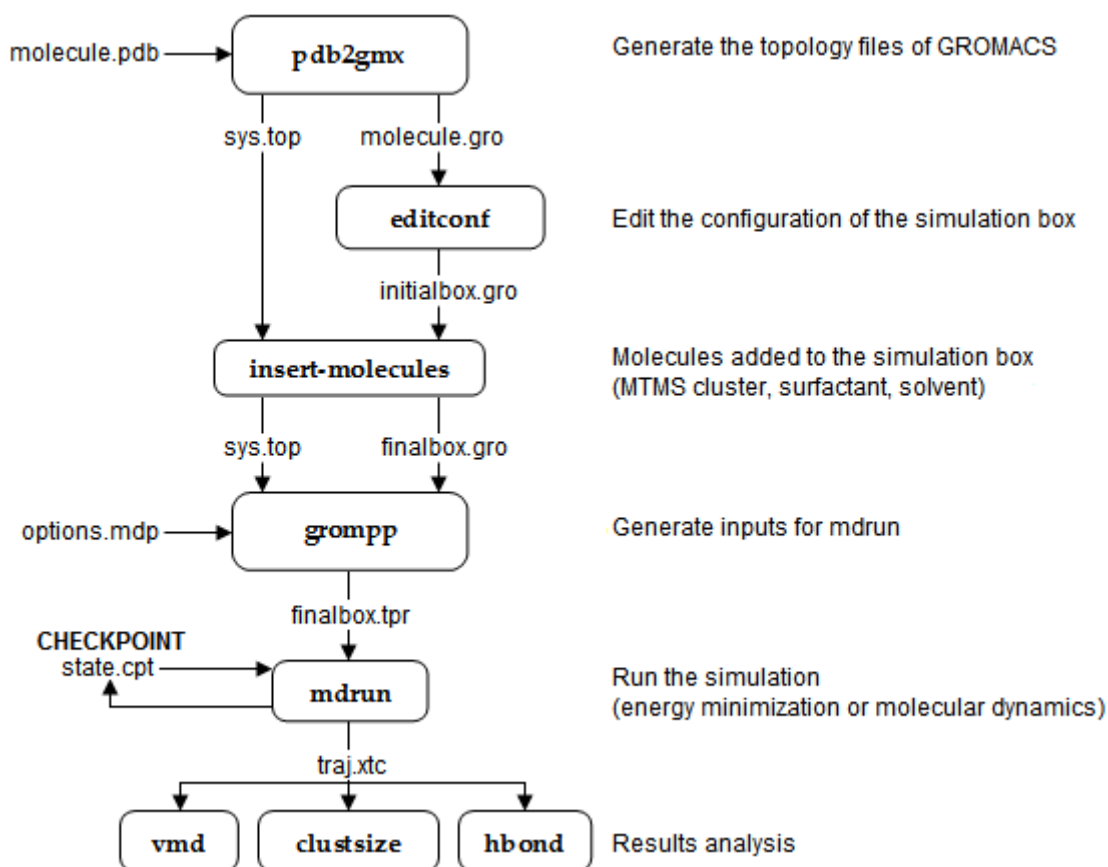
Figure 2.5 - Flowchart for a typical GROMACS MD run of this thesis (adapted from GROMACS – flow chart [30])

Results analysis

There are several possibilities to analyze the obtained MD results. The first and fastest one is to load the trajectories file (traj.xtc), from the simulation, into a program like Visual Molecular Dynamics (VMD), and actually visualize the evolution of the simulation. Nevertheless, this corresponds just to a qualitative assessment of the system, and a more quantitative approach is required. Other possibilities to analyze the data produced in this thesis are to use the command *hbond*, which computes and analyzes hydrogen bonds between molecules, or the command *clustsize* that is able to compute the size distributions of molecular/atomic clusters [31][32]. The *hbond* is used whenever hydrogen bonds are possible to

occur between the precursor particles and the *clustsize* is used in all results due to the natural aggregation of the particles.

2.5.2 MTMS-derived aerogel structures

In sol-gel condensation reactions, MTMS-hydrolyzed species react with one another and form clusters that can be dimmers, trimmers and so on. However, to this date, not many works have been developed that contemplate the possible structures MTMS forms when condensation is occurring [33]. Benvenutti *et al.* (2009) [34] have reported that silsesquioxanes[2] can form three different structures: random, a bidimensional structure that can create a layer arrangement or a ladder shape, and a tridimensional arrangement in cage shape. Kanamori *et al*. (2014) [35] stated that the structures can be random, a perfect cage or a partial cage, but none of these works investigate the most likely structure that a MTMS precursor forms, they just present a generic assessment.

Thankfully, a very recent study, presented in Table 2.10, sheds some light into the most likely conformation for MTMS clusters.

Table 2.10 - Article from literature with interest for the present work, presenting the most likely cluster conformation formed by MTMS [33].

Article	Chemical System	Computational Details	Relevant Conclusions
Borba et al., 2016	MTMS based aerogels	•Approach based on an integrated vibrational frequency prediction within the DFT/B3LYP framework and experimental counterpart; •A total of thirteen different structures were studied by quantum chemical calculations; •Constricted to a maximum of eight Si atoms due to computational constraints; •Harmonic frequency calculations were done to ensure the computed structures corresponded to the minimum on potential energy.	•Theoretical results suggest that cyclic and/or polycyclic structures are more probable than linear ones, meaning that a caged structure is more probable; •Was established a tentative relationship between FTIR spectra and microstructural properties; •The experimental data confirmed the theoretical predictions. (in condensation, linear and cyclic are the dominant structures and after gel point branched and cyclic are the dominant ones).

The structures that were selected for the model used in this work were proposed by Borba *et al.* (2016) [33] as the most probable MTMS-derived structures formed in the early stages of condensation. They are presented in Figure 2.6.

---

[2] Silsesquioxanes - Hybrid inorganic-organic structures with the chemical formula $[RSiO_{3/2}]_n$, being R an organic group.

a)   Cyclic structure with 4 silicon atoms   b)   Cage with 8 silicon atoms
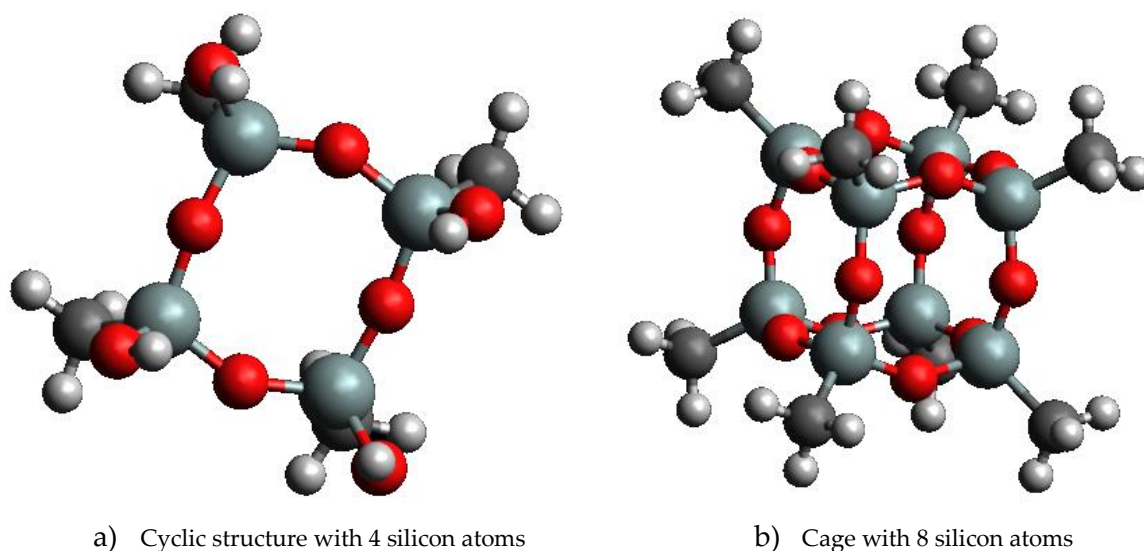
Figure 2.6 - MTMS-derived structures used in this thesis.

These two structures can be compared between them because one is a complete cage and the other, in simple terms, is half of it. For the sake of simplicity, throughout this thesis, the cyclic structure will be named SI4 and the cage structures as SI8. These will be generically designated by "particles".

3   Experimental and computational details

This chapter is divided into three sections. The first section presents a description of the used chemicals, the synthesis of gels with and without surfactant, the drying of the gel and a summary of the synthesized materials. The second section gives details about the characterization of the materials. The third section describes the materials, the computational tools and conditions, the simulation box and a summary of the simulations made and the tools used for results analysis.

3.1   Synthesis of aerogels

3.1.1   Materials

The materials in this work where obtained with the precursor methyltrimethoxysilane (MTMS, $CH_3Si(OCH_3)_3$, $\approx 98\%$), the catalysts oxalic acid ($C_2H_2O_4$, $\geq 99\%$) and ammonium hydroxide (NH_4OH, 25% NH_3 in H_2O), methanol (CH_3OH, $\geq 99.8\%$) as solvent and the surfactants hexadecyltrimethylammonium bromide (CTAB, $CH_3(CH_2)_{15}N(Br)(CH_3)_3$, $\geq 99\%$), sodium dodecyl sulfate (SDS, $CH_3(CH_2)_{11}OSO_3Na$, $\geq 99\%$) and Pluronic F127 (F127, $H(OCH_2CH_2)_x(OCH_2CHCH_3)_y(OCH_2CH_2)_zOH$, $M_n \approx 12600$ Da). All of these were supplied by Sigma Aldrich and used without further purification, and the high purity water was obtained in the *Direct Pure Water System* of *Rephile Bioscience*. The chemical structure of these surfactants is presented in Figure 3.1.

| CTAB | SDS | Pluronic F127 |
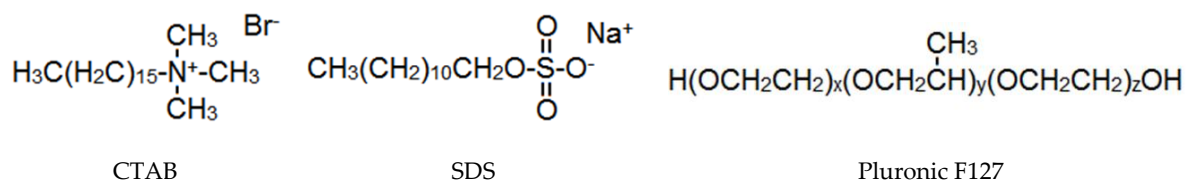
Figure 3.1 - Chemical structures of the surfactants used in this work.

3.1.2   Synthesis of gels with and without surfactant

The synthesis of the MTMS-derived gels, followed a two-step acid-base process similar to the one presented in Durães *et al*.,(2012) [6]. The calculations to define the reagents amounts and ratios for the gel are similar to those presented by Meneses (2014) [36].

All the synthesis were performed with the molar ratios of 1:35:4:4 for MTMS:methanol:acidic water:alkaline water and an amount of surfactant ranging from no surfactant to 1.500 g. The procedure starts with the hydrolysis of MTMS, promoted with the acid catalyst, in a solution of methanol, MTMS, surfactant and acidic water (0.01 M of oxalic acid). This solution is stirred for 30 minutes in a water bath at 27°C. Then the solution is kept inside an oven for 24 hours at 27°C in order to promote the hydrolysis reaction. After this time, the alkaline catalyst (10 M of ammonium hydroxide) is slowly added to the solution to promote the condensation and the subsequent step of gelation. Afterwards, the solution is placed in an oven at 27°C for a period of 48 hours in which gelation occurs and then the gel is aged.

3.1.3   Drying of the gels

After gel aging, the gels were dried using a supercritical fluid drying approach, where CO_2 was used in order to obtain aerogels.

The supercritical drying with CO_2 is performed in two consecutive steps. In the first step, the gel is washed with a solvent, in this case methanol. It drags the chemicals insoluble in supercritical CO_2, mostly the ammonium hydroxide and water. In the second step, supercritical CO_2 is forced to pass through the sample in order to dissolve and drag the methanol, leaving behind the dried silica skeleton that forms the aerogel. The conditions used for this drying method are listed in Table 3.1.

Table 3.1 - Conditions used for supercritical drying with CO_2 [7].

	Pressure (bar)	Flow rate (mL.min^{-1})	Run time (minutes)	Cell temperature (°C)
MeOH	120	2	60	50
CO_2	≈150	3	90	50

3.1.4   Summary of the synthesized materials

This work started using an ambient pressure drying (APD) approach and, as such, producing xerogels. However, as can be seen in Appendix A, the results were not good due to the difficulty of removing the surfactant. Thus, the APD route was abandoned.

The nomenclature of the materials synthesized is done according Table 3.2 where the letter A stands for MTMS aerogel.

Table 3.2 - Nomenclature of the aerogels synthesized with various surfactants and surfactant's amounts.

Sample	Replicas	Surfactant	Surfactant amount (g)
A	LPC-0.0; LPC-0.1; LPC-0.2; LPC-0.3	Without surfactant	---
A_CTAB_0.50	LPC-010; LPC-011; LPC-012; LPC-013		0.50
A_CTAB_0.75	LPC-003; LPC-004; LPC-005; LPC-009		0.75
A_CTAB_1.00	LPC-000; LPC-001; LPC-002	CTAB	1.00
A_CTAB_1.25	LPC-006; LPC-007; LPC-008		1.25
A_CTAB_1.50	LPC-014; LPC-015; LPC-016; LPC-017; LPC-018		1.50
A_F127_0.50	LPC-019; LPC-020; LPC-024; LPC-025; LPC-034		0.50
A_F127_0.75	LPC-030; LPC-031; LPC-032; LPC-035		0.75
A_F127_1.00	LPC-026; LPC-028; LPC-029; LPC-036	Pluronic F-127	1.00
A_F127_1.25	LPC-037; LPC-040; LPC-042; LPC-052		1.25
A_F127_1.50	LPC-041; LPC-043; LPC-045; LPC-050; LPC-053		1.50
A_SDS_0.50	LPC-039; LPC-044; LPC-046; LPC-054	SDS	0.50
A_SDS_0.75	LPC-047; LPC-048; LPC-051; LPC-055		0.75

3.2 Characterization of the synthesized materials

After the synthesis of aerogels, their chemical, physical and mechanical characterization was performed. The techniques here described were chosen.

3.2.1 Chemical characterization

Fourier transform infrared spectroscopy (FTIR)

FTIR allows to assess the chemical structure of the aerogels by identifying the chemical bonds whose vibrations occur in the infrared range. The infrared radiation is not energetic enough for electronic transitions to occur and as such the radiation absorbed causes the

chemical bonds to vibrate more intensely. The absorption occurs when the chemical bond has a dipole moment and interacts with incident infrared radiation. The frequency at which a chemical bond vibrates is unique since it depends on the mass of the atoms and the strength of the bonds involved [37]. Thus, the FTIR spectrum obtained for a sample is a "fingerprint" of the chemical structure under analysis.

The FTIR analysis of aerogels was performed in a *Jasco FT/IR 4200* equipment, in the mid-infrared region, in particular between 4000 and 400 cm^{-1}, with a resolution of 4 cm^{-1}.

In order to analyze the aerogels, pellets were prepared with 78.5 to 80 mg of KBr and 0.20 to 0.30 mg of the material. The pellet was then put inside de spectrometer and a beam of light, in the infrared region, hits the pellet generating a transmission spectrum as a function of wavenumber. This characterization was carried out for each dried sample.

Elemental analysis

The elemental analysis main goal was to determine quantitatively the mass fraction of some chemical elements, specifically C, H, N, S in the aerogel samples. This was determined using the EA 1108 CHNS-O from *Fision Instruments*.

For the determination of the referred elements, the sample was subjected to a flash combustion at 900°C using a flow of He enriched with oxygen. The resulting combustion gases (CO_2, H_2O, N_2 and SO_2) are separated with a chromatographic column and quantified by a thermal conductivity detector that emits a signal proportional to the concentration of the individual components of the sample. The aerogel samples were prepared by mixing replicas of each type of aerogel and grinding them to a fine dust like powder, in order to have a representative sample for the selected aerogels. The aerogels chosen for this analysis were: A, A_CTAB_1.25, A_CTAB_1.50, A_F127_1.25, A_F127_1.50 and A_SDS_0.75. These include the aerogel without surfactant and the ones that presented the best results in terms of bulk density.

Contact angle

Contact angles (θ_c) may give information about the interactions between solid surfaces and liquids, in this case the aerogel and water, and in this way assess if the materials are hydrophobic or not. Silica aerogels are often hydrophobized as they tend to degrade upon exposure to moisture (hydrolysis reactions), thus the measuring of the contact angle is of major importance.

This technique consists in the deposition of a small drop of water over the surface of the material and then the software defines the drop profile and calculates the angle formed through the Young's equation. A typical representation for contact angles >90° is presented in Figure 3.2.
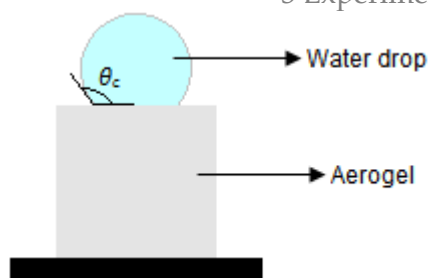
Figure 3.2 - Representation of contact angles above 90°.

The main interactions acting in the system are the cohesive forces between the water molecules and the adhesive forces between the water molecules and the solid surface. When the contact angle is lower than 90° it means that there is an affinity between the liquid and the solid, and the liquid wets the surface which means the material is hydrophilic. However, when the contact angle is higher than 90°, little affinity between the water molecules and the solid surface exists and the cohesive forces prevail, being the material hydrophobic.

The measurement of θ_c was done with *OCA 20* equipment, from *DataPhysics*, and all the synthesized samples had their contact angles evaluated. For each sample 8 to 10 measurements were done in order to have a representative average contact angle.

Zeta potential

Zeta potential is a parameter indirectly determined by the surface charge of solid particles in a colloidal dispersion [38]. It indirectly measures the net electrical charge created in the particles in a suspension, either by adsorption of counter ions or dissociation of surface groups from the particles. The higher absolute values of zeta potential the more stable is the suspension, since the charged particles repel each other which overcomes the tendency to form the aggregates caused by the Van der Waals forces [39].

This technique is used to quantify the charge of the surface of silica particles obtained from the aerogel without surfactant. Experimentally, 0.55 mg of the aerogel sample were ground and dispersed in 2 mL of methanol using an ultrasound bath. Then, this suspension was inserted with a syringe in the sample cell of the *Zetasizer*, from *Malvern Instruments*, and the measurement was run. Only sample A was measured but the measurements were replicated five times.

3.2.2 Physical/Structural characterization

Bulk density

Bulk density (ρ_b) is the ratio between the mass and the volume of a sample and is obtained by taking into account the total volume of the material including the pore volume.

This is an important characteristic to evaluate in aerogels, since there is a relation between this property and the extent of porosity and, thus, their thermal conductivity.

To measure this property, the samples were cut in a cuboid shape, weighed in a high precision scale and measured with a micrometer. The obtained values for each sample were then calculated according to the Equation 3.1.

$$\rho_b = \frac{m}{V_b} \tag{3.1}$$

All samples were characterized and 4 separate measurements for each replica were made in order to achieve an average value.

Helium pycnometry

Helium pycnometry allows to determine a good approximation to the real volume of the solid material and its global porosity. It uses an inert gas with small molecule size, in this case helium, which fills all the pores of the material. A small portion of a sample is ground to a fine powder and then is put in a chamber where helium is injected until it occupies all the free space. The pressure is measured in the same chamber. Then, by opening a valve that connects this chamber to a secondary chamber, the helium expands to the latter and the pressure at equilibrium is again measured. Thus, by considering the pressure difference it is possible to calculate the volume of the solid matrix - skeletal density [40].

The equipment used to measure this property was an *Accupyc 1330* from *Micrometrics* and the analyzed samples were A, A_CTAB_1.25, A_F127_1.25 and A_SDS_0.75.

By using the bulk and skeletal densities it is possible to estimate the porosity of the material with Equation 3.2.

$$\epsilon(\%) = \left(1 - \frac{\rho_b}{\rho_s}\right) \times 100 \tag{3.2}$$

Scanning electron microscope (SEM)

SEM is a technique that provides information on the morphology, size and appearance of the structural units in the material by generating images of the materials surface.

This technique is performed while scanning the sample's surface, under vacuum, with a focused electron beam. The beam interacts with the atoms in the sample, originating the emission of secondary electrons, backscattered electrons and also the emission of characteristic x-rays. With the detection of the secondary electrons (atom's outer shell electrons), the equipment can generate images of the sample's surface features. On the other hand, with the detection of the backscattered electrons (elastically scattered primary electrons from the beam) and the characteristic x-rays, it is possible to obtain chemical information about the sample. For the detection of the characteristic x-rays the microscope needs an Energy-dispersive x-ray spectrometer detector (EDS). The x-rays generated in the sample are resultant from the relaxation of excited electron states generated by inelastic interaction of the beam with inner-shell electrons of the sample's atoms. As the silica aerogels are not electrically conductive, it is

necessary to coat the sample with a thin layer of gold, so that the electrons from the beam do not accumulate on the sample and hinder the observation. This is done by physical vapor deposition (PVD) during 15 s.

The observed samples were A, A_CTAB_0.75, A_CTAB_1.25, A_CTAB_1.50, A_F127_0.75, A_F127_1.25, A_F127_1.50 and A_SDS_0.75 which were put inside a *ZEISS MERLIN Compact/VPCompact, Field emission scanning electron microscope (FESEM)*, over a metallic sample holder.

Accelerated surface area and porosimetry (ASAP)

The ASAP technique was used to obtain the specific surface area and the pore size distribution of the best aerogels. It uses gas sorption with N_2 in order to determine the surface area but it can also give, indirectly, the pore size distribution. The sorption can be a physical process, in which the adsorbate molecules interact with the adsorbent by Van der Waals forces, or a chemical one, where the molecules bond to the surface of the adsorbent, with covalent or ionic bonding. This technique is based on the increase of N_2 pressure inside a chamber with the sample, starting from very low relative pressure ($P/P_0 < 0.05$; $P_0 -$ Saturation pressure), enabling the sorption of the test gas molecules onto the solid surface of the sample and allowing to measure the equilibrium pressure at which all surface is covered with a single layer of gas molecules (monolayer). By knowing the amount of gas sorbed in the monolayer and the mean surface area of each gas molecule, with the application of the Brunauer-Emmett-Teller (BET) theory, it is possible to calculate the surface area of the material. The pore size distribution of the sample is determined using the algorithm of Barret, Joyner, Halenda (BJH) by the application of the Kelvin and the Halsey equations [41].

All samples were previously degassed during three days at 50°C, in a vacuum oven, and also degassed in the equipment at 80°C until pressure stabilization. The equipment used to evaluate the surface area and pore size distribution of aerogels was an *ASAP 2000*, from *Micromeritics*, and the samples tested were A, A_CTAB_1.25, A_F127_1.25 and A_SDS_0.75.

3.2.3 Mechanical characterization

Compression test

The uniaxial compression test was used to determine the Young's modulus of the synthesized aerogels when the test sample is subjected to an external uniaxial compression force.

Materials may suffer strain of two types. One is when the material has the capability of recovering its initial shape, called elastic strain, and the other is when the material is not able to recover its initial shape, being permanently deformed, which is named plastic strain.

The Young's modulus is determined through Equation 3.3, where σ stands for the stress and ε is the strain. This equation is obtained from the Hooke's Law, which states that stress is linearly proportional to the strain, when the specimen is under elastic deformation. The proportionally constant is the Young's modulus and corresponds to the slope of the stress-strain curve in the elastic region (initial linear part of the curve).

$$\text{Young's modulus } (E) = {}^{\sigma}\!/_{\varepsilon} \tag{3.3}$$

The compression tests were performed on a *Shimadzu Autograph AG-X* machine and only one replica of each sample was tested. The tested replicas belonged to samples A, A_CTAB_1.25, A_F127_1.25 and A_SDS_0.75. The tests were conducted up to 50% strain of the test sample with a deformation rate of 10 mm.min^{-1}. It is worth mentioning that all samples recovered completely their original size after the test.

3.3 Computer simulation of the aerogels structure

3.3.1 Materials

The primary structures of the MTMS-derived species used in the simulations were the SI4 and SI8 particles that were presented in the subsection 2.5.2. The remaining components used in the simulations were the solvent molecule, methanol, and the surfactant CTAB.

In order to have a representative sample, several quantities of the MTMS-derived particles SI4 and SI8 were simulated. For the surfactant, the smallest quantity experimentally tested and the quantity considered as optimal for achieving the lower bulk density were simulated, in order to analyze the possible differences resulting from the addition of surfactant.

The FF of these species, as explained in section 2.5, were obtained through the ATB database.

3.3.2 Computational tools

This thesis uses the Ubuntu operating system (OS) with the GROMACS package in order to run molecular dynamics on a system composed of MTMS-derived particles, methanol and surfactants. The Visual Molecular Dynamics (VMD) allows the visualization of the simulation boxes and the creation of movies. The Grace is a free graph plotting tool of the Ubuntu OS and was used for plotting the results obtained with the *clustsize* and *hbond* commands.

3.3.3 Computational conditions

The computer simulations were conducted at the same ambient P-T conditions of gelation, however the pH was considered 7 and, as such, different from the condition used in the laboratory for condensation, where the pH is normally in the range of 10-12. The main reason for this difference was that the change in pH introduces a new variable, which can only be tuned by adding of new ionic species, turning the system more complex and requiring more computation time. For the present work the pH variable is not as important as the assessment of the effect of different surfactants in the clustering process of the system.

3.3.4 Simulation box

All simulations started by generating the molecules topology files. The building of the simulation box begins with the creation of a box with 10 nm^3 and then by randomly adding the species by the order shown in Figure 3.3.
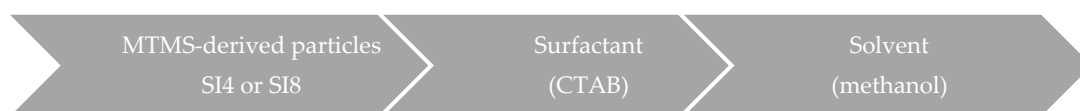
Figure 3.3 - Flow diagram of the species added into the simulation box.

The reason for this order is related with the components amounts/molar ratios. Both in the laboratorial and computational work, the number of methanol molecules inserted in the box was much larger than the number of MTMS-derived particles or surfactant molecules, making easier to add them at the end. A different order could, however, be used and it probably would not have much effect on the final result. For a better understanding on the molar ratios and how much particles are involved in the simulation see Appendix B.

Once all the basic particles required to perform the simulation are inserted into the box, an energy minimization is performed. This is done to relax the system and for not blowing it up, because one molecule would shoot away due to an accumulation of potential energy and momentum, as soon as the calculation of trajectories would start.

The trajectory calculations begin by running the output of the minimum-energy system. These were simulated for 80 ns, with 2 fs per steps.

3.3.5   Summary of the simulations made

The nomenclature of the simulations performed in this work is presented in Table 3.3.

Table 3.3 - Summary of the simulations made.

Simulation	MTMS-derived particle	Number of MTMS-derived particles	Surfactant	Surfactant quantity (g)
B1		90		
B2		80	---	---
B3		70		
B1_CTAB0.50		90		
B2_CTAB0.50	SI4	80		0.50
B3_CTAB0.50		70	CTAB	
B1_CTAB1.25		90		
B2_CTAB1.25		80		1.25
B3_CTAB1.25		70		
C1		45		
C2		40	---	---
C3		35		
C1_CTAB0.50		45		
C2_CTAB0.50	SI8	40		0.50
C3_CTAB0.50		35	CTAB	
C1_CTAB1.25		45		
C2_CTAB1.25		40		1.25
C3_CTAB1.25		35		

3.3.6   Tools for results analysis

VMD

Visual molecular dynamics or VMD is the tool used to visualize the simulation box and the computed trajectories. In simple terms, this is done by writing the following command "vmd (insert name of the simulation).gro". To see the trajectories it is required to use the output .xtc that holds the trajectories of each individual molecule.

This tool was used to visualize all the computed systems.

hbond

The *hbond* command in GROMACS computes and analyzes hydrogen bonds [31]. More specifically, it computes the donor and acceptor of hydrogens (OH and O, respectively). This was applied only to the systems containing SI4 particles because these have donors of hydrogens while the SI8 particles do not. Thus, with this command the goal was to see if the

MTMS precursor has a tendency to aggregate into cage-like structures through hydrogen bonding.

In order to calculate the number of hydrogen bonds an index file was used (the same as in the *clustsize* command) but this time the command was "gmx hbond (insert name of the simulation).xtc".

clustsize

The *clustsize* command provided by the GROMACS package computes the size distributions of molecular clusters [32], meaning that, in this case, it computes the aggregates of SI4 or SI8 particles. This is done using an index file where the several molecules are discriminated and, then, by typing "gmx clustsize (insert name of the simulation).xtc" on the command line of the console.
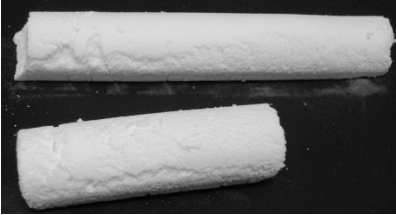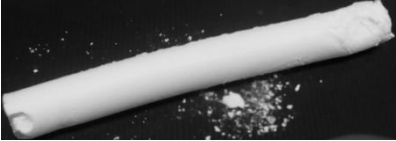
This command was used in all the simulated systems.

4 Results and discussion

4.1 Samples and laboratory observations
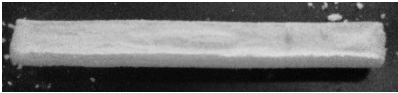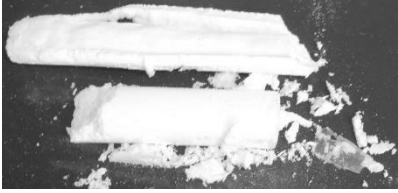
Table 4.1 presents a photo, the observable results and the bulk density of the different synthesized samples.

Table 4.1 - Pictures, observable characteristics and bulk density of the synthesized aerogels.

Sample	Photo	Observations	ρ_b (kg.m^{-3})
A		Complete gelation. Supernatant present. Easily dried. Powdery, opaque and flexible.	53.2 ± 7.9
A_CTAB_0.50		Complete gelation. Supernatant present. Easily dried, Powdery, opaque and flexible.	54.4 ± 3.8
A_CTAB_0.75		Complete gelation. Supernatant present. Easily dried. Powdery, opaque and flexible.	49.4 ± 4.5
A_CTAB_1.00		Complete gelation. Easily dried. Powdery, opaque, very flexible and slightly bent.	47.5 ± 3.0
A_CTAB_1.25		Complete gelation. Perfect monolith. Easily dried. Opaque and more flexible than sample A	43.9 ± 2.3
A_CTAB_1.50		Complete gelation. Perfect monolith. Hard to dry (needs more time). Opaque and more flexible than sample A.	44.1 ± 1.8
A_F127_0.50		Partial gelation. Easily dried. Supernatant present. Sample adheres to the glass tube. Deposition of the silica species. Opaque, powdery and particles shed.	55.6 ± 3.3
A_F127_0.75		Complete gelation. Easily dried. Supernatant present. Sample adheres to the glass tube. Deposition of the silica species. Opaque, powdery and particles shed.	56.2 ± 3.9

Table 4.1 – Pictures, observable characteristics and bulk density of the synthesized aerogels. (Cont.)

Sample	Photo	Observations	ρ_b (kg.m^{-3})
A_F127_1.00		Complete gelation. Easily dried. Supernatant present. Sample adheres to the glass tube. Deposition of the silica species. Opaque and flexible.	53.7 ± 7.7
A_F127_1.25		Complete gelation. Easily dried. Supernatant present. Sample adheres to the glass tube. Deposition of the silica species. Opaque and flexible.	49.4 ± 3.1
A_F127_1.50		Complete gelation. Easily dried. Supernatant present. Sample adheres to the glass tube. Deposition of the silica species. Opaque, very powdery and flexible.	51.7 ± 3.5
A_SDS_0.50		Complete gelation. Perfect monolith. Hard to dry (needs more time). Opaque and more flexible than sample A	47.4 ± 2.6
A_SDS_0.75		Complete gelation. Perfect monolith. Hard to dry (needs more time). Opaque and more flexible than sample A	45.3 ± 3.6

The information in Table 4.1 allows for a preliminary analysis about the most promising synthesized samples. The samples obtained when using the chosen synthesis method are all opaque. Some laboratory observations made alongside the bulk density characterization of the obtained materials were considered to determine when the amount of a particular surfactant was still advantageous. The samples' dryability was an immediate reference point to whether it was worth continuing to add surfactant in the synthesis process or not. In addition, the apparent flexibility of the material also had an impact when choosing the most promising samples.

At a first visualization, the best samples would be A_CTAB_1.25, A_CTAB_1.50, A_F127_1.00, A_F127_1.25 and both samples with SDS. As these were very flexible, exhibited good monolicity and featured very little particle shedding. However, this analysis by itself is insufficient to validate this selection.

In order to get a better understanding of the samples selection, the average results for the bulk density, with the respective confidence interval at 95%, can be seen in Figure 4.1 with some brief comments afterwards.
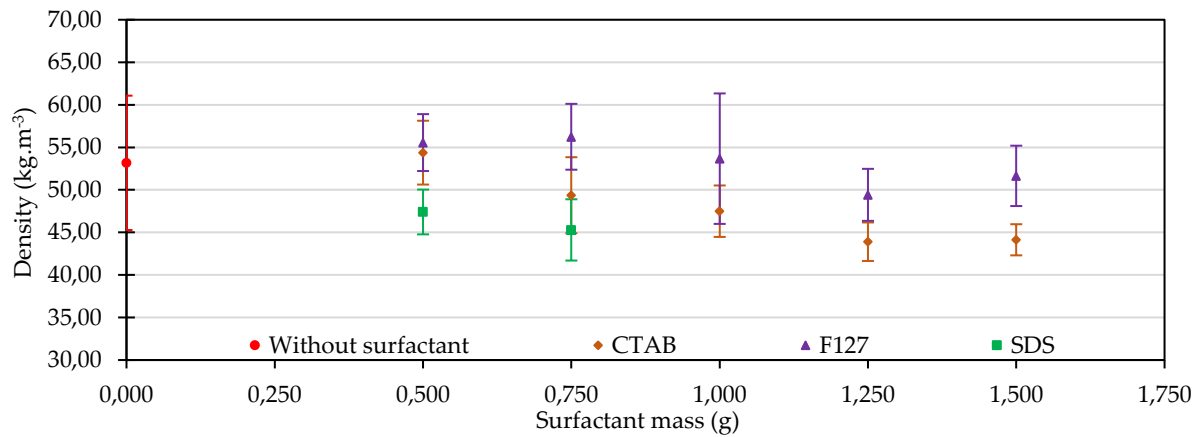
Figure 4.1 - Average bulk density for the synthesized materials with and without surfactant.

Overall, for each surfactant a minimum bulk density was achieved. For the CTAB and F127 this minimum was when 1.250 g were added and for the SDS the minimum was observed at 0.750 g. These minima were considered in the selection of the best samples, since the lower is the bulk density the better are the materials for thermal insulation, according to the known expression $k \propto \rho^{1.5}$ [42]. For SDS samples, the obtained values tend to decrease with the increasing mass of surfactant. Thus, the minimum bulk density was considered for the last value. In this case, higher amounts of surfactant led to non-dried samples. Thus the best samples were A_CTAB_1.25, A_F127_1.25 and A_SDS_0.75. In addition, sample A was also selected for comparison and, in some cases, samples A_CTAB_1.50 and A_F127_1.50 were also analyzed as the extreme cases of surfactant amount. Nevertheless, for some more accessible analysis techniques, all the synthesized samples were assessed.

4.2 Chemical characterization of the aerogels

4.2.1 Fourier transform infrared spectroscopy (FTIR)

In order to analyze the chemical structure of the different samples, the infrared spectroscopy was used, as referred in the previous chapter. The FTIR results are presented in three figures (Figures 4.2-4.4), one for each surfactant (consult Appendix C for more information). The results will be briefly discussed as they are presented and afterwards a summary regarding the FTIR analysis is made.

Figure 4.2 - FTIR spectra of the pure MTMS-derived aerogel and the MTMS-derived aerogels with the cationic surfactant, CTAB (ν-stretching vibrations, ν_s-symmetric stretching vibration, ν_{as}-antisymmetric stretching vibration, ν_β-in-plane stretching vibration, δ-deformation vibration, δ_s-symmetric deformation vibration (bending), δ_{as}-antisymmetric deformation vibration (bending)).

Through the observation of Figure 4.2, it is possible to verify that all the samples have similar spectra, thus a similar chemical structure. The first peak, visible at 421 cm^{-1}, corresponds to the deformation vibration of the O-Si-O bond. The peaks of the Si-O bonds also appear at 549, 676 and 771 cm^{-1}, which correspond to the symmetric stretching vibrations, and at 920 cm^{-1}, which is the in-plane stretching vibration. At wavenumbers of 1000-1100 cm^{-1}, the antisymmetric stretching vibrations of the Si-O-Si bonds are evident [37][43].

The presence of a peak at 835 cm^{-1} is indicative of the existence of the methyl functional groups linked to Si, representing the stretching vibrations of Si-C bonds.

The peaks visible between 2850-2970 cm^{-1} represent the symmetric and antisymmetric stretching vibrations of C-H bonds. The presence of these is indicative of the hydrophobicity of the material, because they are characteristic of the -CH$_3$ groups from the MTMS precursor.

The peaks at 1270 cm^{-1} and at 1400-1460 cm^{-1} indicate the symmetric and antisymmetric deformation vibrations of the C-H bonds for the -CH$_3$ and Si-CH$_3$ groups.

In one of the samples (A_CTAB_1.50), it is also possible to identify the presence of a probable contamination, giving an indication of C=O bonds that should not be in this system.

By the observation of Figure 4.2, the similarity of the FTIR spectra for all the samples shows not only that a silica structure is formed in all of them but that there is also no surfactant present in the final structure because no discernible characteristic bands of tertiary amines (corresponds to C-N bonds) are present in the spectra (namely bands at 1000-1250 cm^{-1}). This may be due to the presence of strong peaks for other structural units in the same region, but since the overlapping of peaks usually results in shoulders in the spectra it is safe to assume that no surfactant seems to be present.
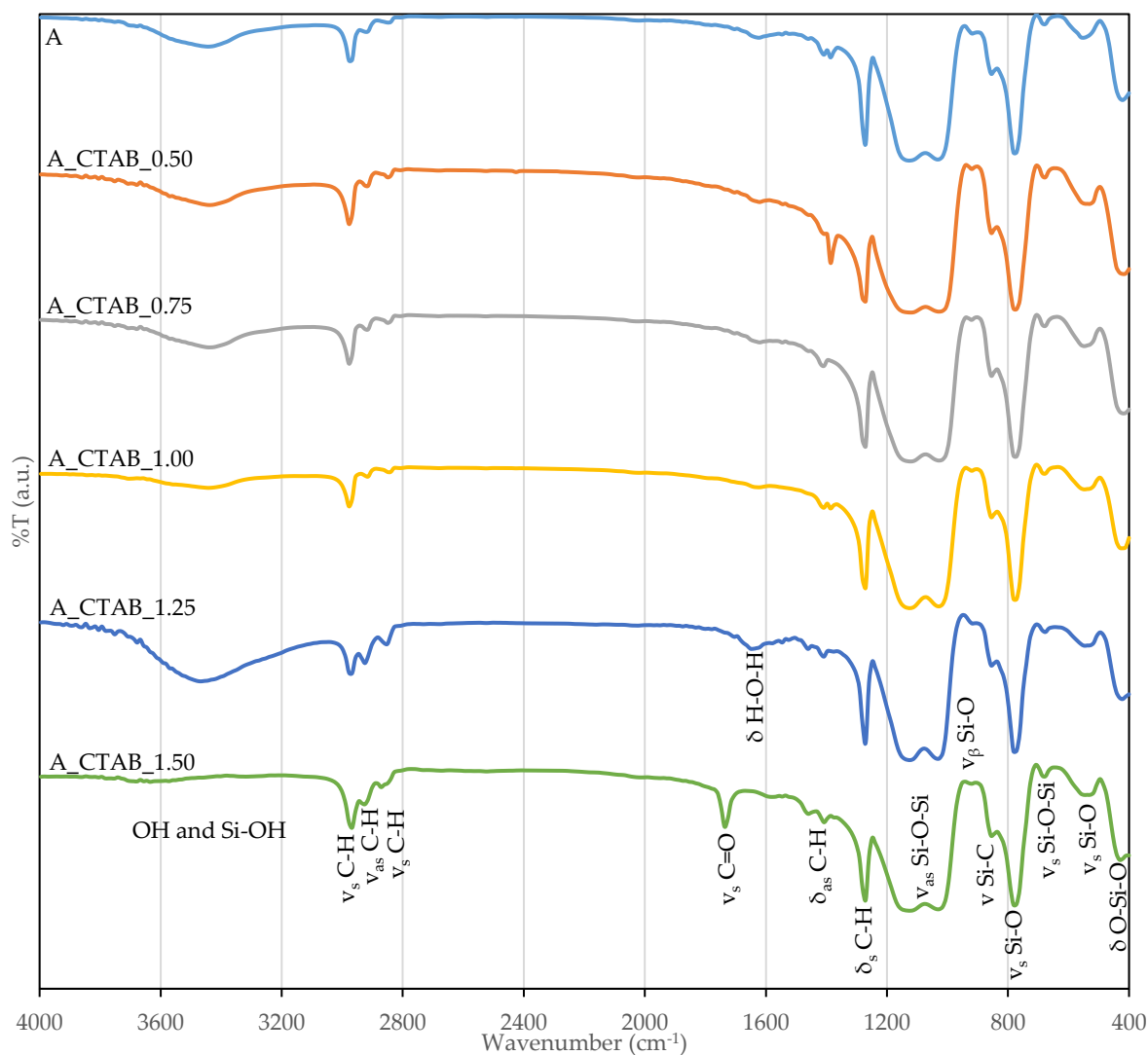

Figure 4.3 - FTIR spectra of the pure MTMS-derived aerogel and the MTMS-derived aerogels with the nonionic surfactant, F127 (v-stretching vibrations, v$_s$-symmetric stretching vibration, v$_{as}$-antisymmetric stretching vibration, v$_\beta$-in-plane stretching vibration, δ-deformation vibration, δ$_s$-symmetric deformation vibration (bending), δ$_{as}$-antisymmetric deformation vibration (bending)).

41

In Figure 4.3, the same bonds are seen as in Figure 4.2, leading to the previously stated conclusions. There also seems to be a small peak (corresponding to the C=O bond) in the sample A_F127_0.50 which could be a contamination.

It is also possible to see that the spectra are all similar between them, but the location of the possible peaks that could indicate the presence of F127 in the dried structure coincide with the bonds that correspond to the CH_3 groups present in the pure sample A, thus it is not possible to ascertain with 100% confidence that no F127 remained in dried structure.
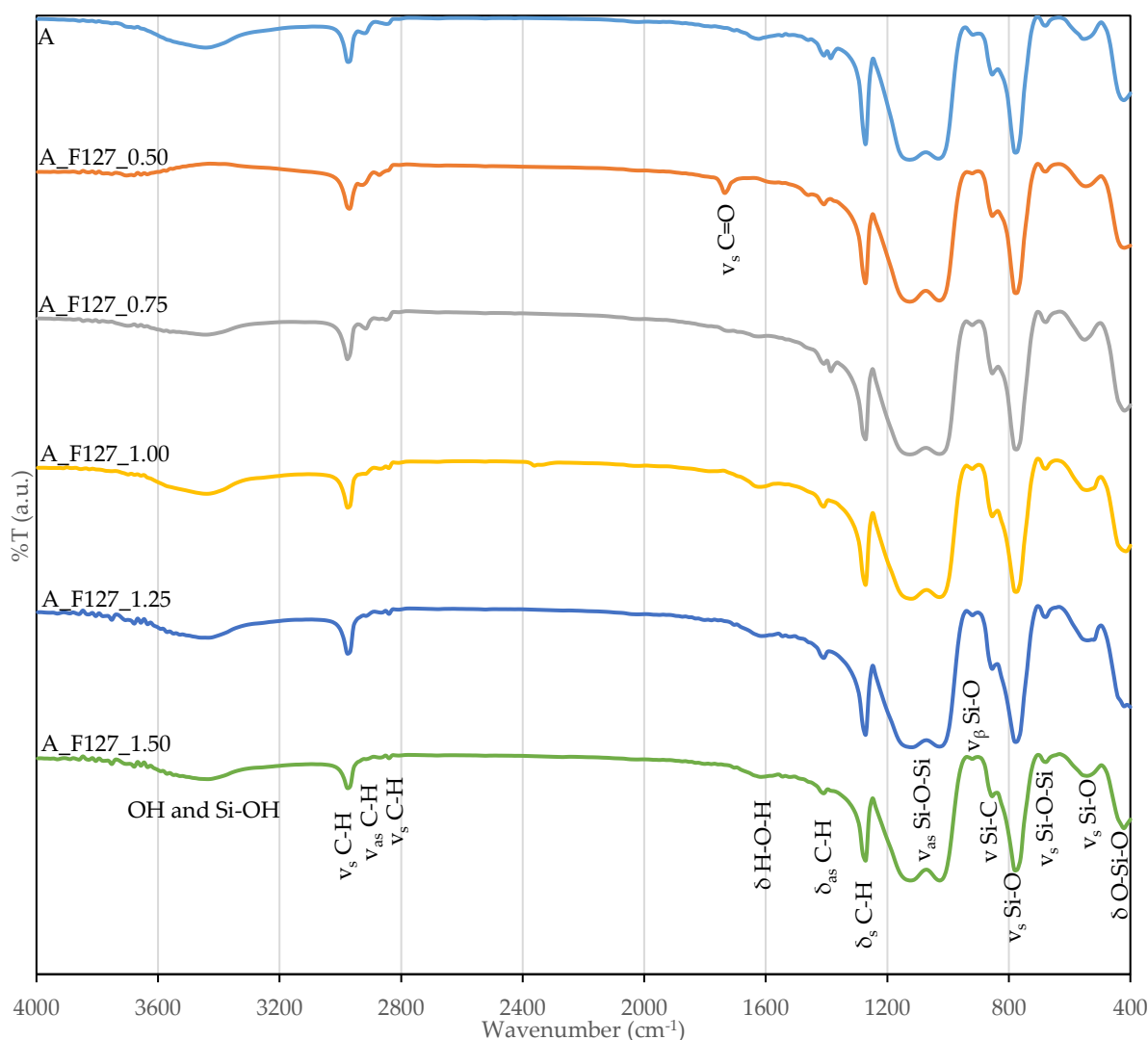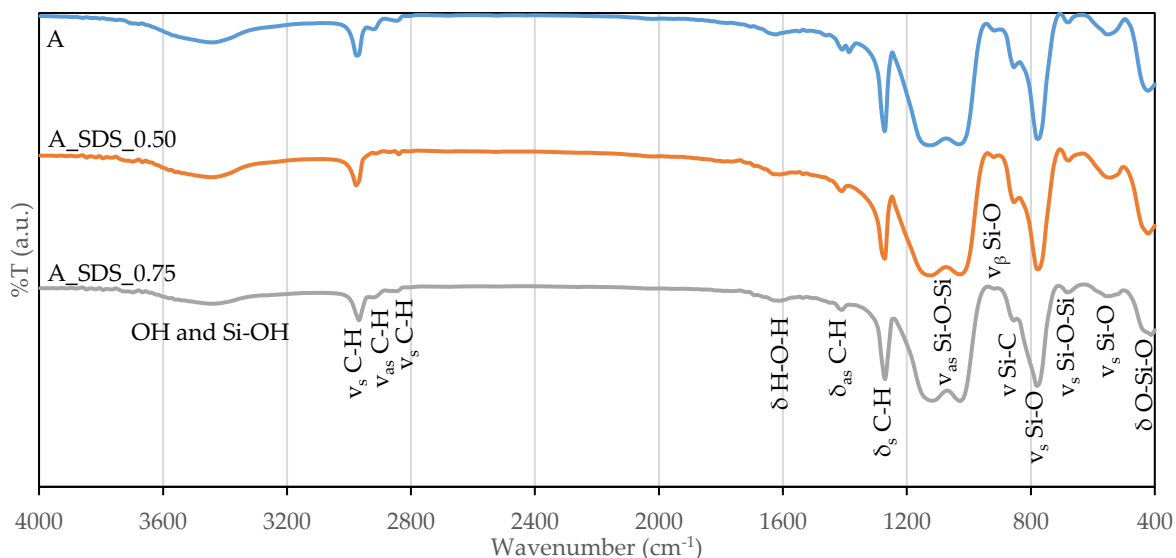

Figure 4.4 - FTIR spectra of the pure MTMS-derived aerogel and the MTMS-derived aerogels with the anionic surfactant, SDS (v-stretching vibrations, v_s-symmetric stretching vibration, v_{as}-antisymmetric stretching vibration, v_β-in-plane stretching vibration, δ-deformation vibration, $δ_s$-symmetric deformation vibration (bending), $δ_{as}$-antisymmetric deformation vibration (bending)).

By observing Figure 4.4, there is no peak that could possibly indicate the presence of contaminants, the spectra are similar as in Figures 4.2 and 4.3. In addition, there is no obvious trace of the SDS surfactant. This may be because the peak that indicates the presence of SO_4^- is near 1100 cm^{-1} which coincides with the major peaks corresponding to the Si-O-Si bond. Moreover, the zone of C-H bonds does not have significant changes, thus making impossible to identify its presence solely through this characterization.

It is worth mentioning that the base line for each spectrum is not equally leveled in order to comment the size difference in the peaks of the spectrums and relate it to the samples' amount.

When taking into account the three previous figures, it is not possible to detect the presence of surfactant in the dried structure, the spectra being all quite similar in terms of the visible characteristic peaks. Thus, the used surfactants were well removed from the aerogels structure in the drying stage with supercritical CO_2. Also, since all spectra do not present a

peak and/or deviation indicating the presence of ammonia, it seems that base catalyst residuals are not present, meaning that the samples were well dried.

4.2.2 Elemental analysis

This analysis was made in order to determine quantitatively the mass fraction of nitrogen (N), sulfur (S), carbon (C) and hydrogen (H) in the samples. The discussion of these results is organized in two separate steps. In the first one, a brief comment on the obtained results is presented and, in the second, a comparison with the theoretical expected results for complete and incomplete gelation is made.

The results obtained for the elected samples are found in Table 4.2.

Table 4.2 - Experimental mass percentages of CHNS obtained for the selected aerogel samples.

Sample	% C (w/w)	% H (w/w)	% N (w/w)	% S (w/w)	% Si + % O (w/w)
A	18.912	4.675	≤ 100 ppm	≤ 100 ppm	76.413
A_CTAB_1.25	18.580	4.924	≤ 100 ppm	≤ 100 ppm	76.496
A_CTAB_1.50	20.280	5.020	0.100	≤ 100 ppm	74.600
A_F127_1.25	20.156	5.272	≤ 100 ppm	≤ 100 ppm	74.572
A_F127_1.50	21.614	5.405	≤ 100 ppm	≤ 100 ppm	72.981
A_SDS_0.75	18.549	4.628	0.020	≤ 100 ppm	76.803

Through Table 4.2 it can be seen that no sulfur is present in the tested samples, not even in the A_SDS_0.75 aerogel. In fact, in the studied system, sulfur is only present in the SDS molecule but it does not show in the aerogel sample synthesized with this surfactant, proving that the surfactant was effectively removed by $scCO_2$, as already observed in the FTIR results discussion. Nitrogen is present in the samples A_CTAB_1.50 and A_SDS_0.75, which is consistent with the fact that the corresponding gels were very hard to dry. The presence of non-negligible amount of the alkaline catalyst in these gels is due to the hydrogen bonding of ammonium hydroxide with the heads of these surfactants. The residual ammonium hydroxide will retain water in the gel structure, making the gels hard to dry because water is not soluble in supercritical CO_2 ($scCO_2$). Moreover, the aerogel A_CTAB_1.50 may also have retained some residual CTAB (due to the higher amount of added), which also has N in its constitution. However, the presence of nitrogen in these samples was not perceptible in the respective FTIR spectra, probably because of the overlapping of vibration bands.

By analyzing the results of the samples with CTAB and F127, in Table 4.2, the percentages of C and H increase with increasing amounts of surfactant. When comparing these samples with sample A (without surfactant), it is also noticeable that, in general, the C and H

percentages are higher. This observation indicates that some residual surfactant may have not been removed during drying, with the exceptions of samples A_SDS_0.75 and A_CTAB_1.25.

The experimental values obtained for carbon and hydrogen, in this test, are now compared with the theoretical values calculated based on structure assumptions. This comparison allows for a more rigorous explanation on why there are small variations on the percentages of C, since these variations can be related with the extension of the condensation reactions.

The theoretical values are calculated using the hypothetical chemical structure of the MTMS-derived aerogels. Therefore, two different scenarios are assumed: the first scenario, corresponds to a complete condensation, where each existing silicon atom (Si) is bonded to a methyl group (-CH$_3$) and three oxygens (O), which in turn are also bonded to other silicon atoms - since these oxygens are shared, each Si atom corresponds to 1,5 oxygen atoms; the second scenario considers an incomplete condensation meaning that each Si atom is bonded to a methyl group, two shared oxygens and one non-shared hydroxide (-OH) group. Without surfactant, the elements that are present in the skeleton are only Si. O, C and H. In Table 4.3 the theoretical mass percentages calculated for the elements C, H and Si + O are presented.

The performed calculations can be found on Appendix D. For this calculus, the hydroxyl groups remaining at the end of the structure were not taken into account.

Table 4.3 - Theoretical elemental mass percentages calculated for MTMS-derived aerogels.

Scenario	Aerogel	% C (w/w)	% H (w/w)	% Si + % O (w/w)
Complete Condensation	MTMS	17.9	4.5	77.6
Incomplete Condensation		15.8	5.3	78.9

It can be seen in Table 4.3 that the theoretical mass percentage of carbon is lower when compared to the experimental values. This means that the complete condensation scenario is the most likely, but it also indicates the presence of residual surfactant in the final material. Indeed, the used surfactants have a C chain with not less than 10 carbons in the chain. Again, the residual surfactant was not detected by FTIR in Figures 4.2, 4.3 and 4.4. The highest values of % C were observed in samples A_CTAB_1.50 and in F127 samples, suggesting a higher retention of the surfactant in the aerogel's structure.

The % H follows the same trend observed in the % C values. Samples A, A_CTAB_1.25 and A_SDS_0.75 show values that support the complete condensation hypothesis. The remaining samples show values more close those of incomplete condensation and/or had some surfactant entrapped inside the silica structure. Since the surfactant can also prevent the

growth of the silica structure, leading to a more incomplete condensation, the increase in the % H supports this claim, but the two effects may overlap.

At this point, some conclusions can be drawn. It is likely that some ammonium hydroxide remained in the samples A_CTAB_1.50 and A_SDS_0.75, making them harder to dry. All aerogel samples show a % C consistent with the complete condensation hypothesis, but the increase of the % C in the samples prepared with surfactant when compared to the value in sample A evidences that residual surfactant remains in the aerogels after drying.

4.2.3   Contact angles

The contact angles were measured with water in order to evaluate the hydrophobicity of the samples. The obtained results, accompanied with the respective confidence interval at 95%, can be seen in Table 4.4.

Table 4.4 - Contact angles with water for the MTMS-derived aerogels with and without surfactant.

Sample	Average θ_c (°)
A	136 ± 6
A_CTAB_0.50	148 ± 6
A_CTAB_0.75	149 ± 13
A_CTAB_1.00	141 ± 10
A_CTAB_1.25	143 ± 10
A_CTAB_1.50	141 ± 9
A_F127_0.50	142 ± 8
A_F127_0.75	140 ± 4
A_F127_1.00	141 ± 3
A_F127_1.25	141 ± 3
A_F127_1.50	142 ± 7
A_SDS_0.50	138 ± 9
A_SDS_0.75	137 ± 6

Based on the presented results, all samples are highly hydrophobic, with contact angles well above 90°. It confirms that the MTMS precursor forms hydrophobic structures, as expected, due to the presence of methyl groups in the network. These groups are non-polar and have no affinity for water molecules, which are polar. As such, the adsorption of the water molecules into the silica structure is disfavored.

The presence of the surfactant, as seen in Table 4.4 and considering the confidence intervals, seems to cause an apparent tendency to make the structure slightly more hydrophobic, with the values practically constant around 141°. This suggests a rearrangement of the MTMS-derived methyl groups in the silica structure due to the presence of the surfactants. The non-polar chains in the surfactants and the methyl groups have affinity for

one another and align themselves in order to reach a lower energy state during the gelation step. This can lead to a better distribution of the methyl groups in the structure. Moreover, the presence of the surfactant also may lead to non-separation of phases, regulating the pores sizes. This may also have an effect in the values of the contact angle if the porous structure becomes more regular with thinner pores. Overall, it can be said that the moisture of the environment is not a problem for the stability of the prepared aerogels, as they will not degrade upon exposure to water-containing environments.

4.2.4   Zeta potential

This technique was employed in order to assess the surface charge of the MTMS-derived aerogels and to theoretically ascertain which type of surfactant could be the most promising one in terms of interactions in the gelation medium. The result obtained for the pure sample, with the respective confidence interval at 95%, is **-9.25 ± 1.46 mV**.

The achieved result shows that the MTMS-derived particles are negatively charged in their surface. This means that the cationic surfactant, CTAB, has electro-chemical attraction for the MTMS-derived aerogel. This possibly allows, in conjunction with the non-polar affinity already discussed, a greater structuration of the silica network.

The anionic surfactant, SDS, would be repelled by the net charge of the MTMS-derived species, but since it also has a hydrocarbon chain, the methyl groups would still have some affinity for the surfactant. Thus, some degree of structuration is still expected to be seen.

The nonionic surfactant, F127, should just work with the non-polar affinity of the involved species.

4.3   Physical/Structural characterization of the aerogels

4.3.1   Porosity

The results for the bulk density and the helium pycnometry (skeletal density) are analyzed together because they complement each other. The bulk density values for all the samples were already presented in section 4.1. The bulk and the skeletal density allow the calculations of the porosity of the material, by the formula presented in subsection 3.2.2. Table 4.5 summarizes the skeletal density values of the selected samples and the respective porosity.

Table 4.5 - Skeletal density and porosity for selected samples, with the standard deviation.

Sample	ρ_s(kg.m^{-3})	ϵ (%)
A	1036 ± 78	94.9
A_CTAB_1.25	1110 ± 47	96.0
A_F127_1.25	1150 ± 123	95.7
A_SDS_0.75	1280 ± 176	96.5

It can be verified in Table 4.5 that the porosity reaches higher values for samples A_CTAB_1.25, A_F127_1.25 and A_SDS_0.75 with 43.9, 49.4 and 45.3 kg.m^{-3} of bulk density respectively (see section 4.1), than for the sample without surfactant (53.2 kg.m^{-3} of bulk density). The porosity results show an average increase of 1% when compared with sample A.

This was expected, as the bulk density had minimum values for these selected samples with surfactant. Moreover, the lowest bulk density was achieved in the case of addition of CTAB. This result validates the already established idea that CTAB should theoretically be the surfactant to use in order to achieve the better results in terms of structuration of the silica network.

Based on porosity values, it can be said that the surfactant clearly supplies a rearrangement in the structure because the overall bulk density is reduced in the presence of a surfactant.

4.3.2 SEM

With SEM analysis a deeper knowledge on the silica microstructure can be achieved. The chosen samples were observed in different magnifications, 1000x, 10000x and 25000x. However, here, only the lowest and highest magnifications will be presented. Figures 4.5, 4.6, 4.7 and 4.8 present the different SEM micrographs obtained for sample A, the samples with CTAB, the samples with F127 and the sample with SDS.
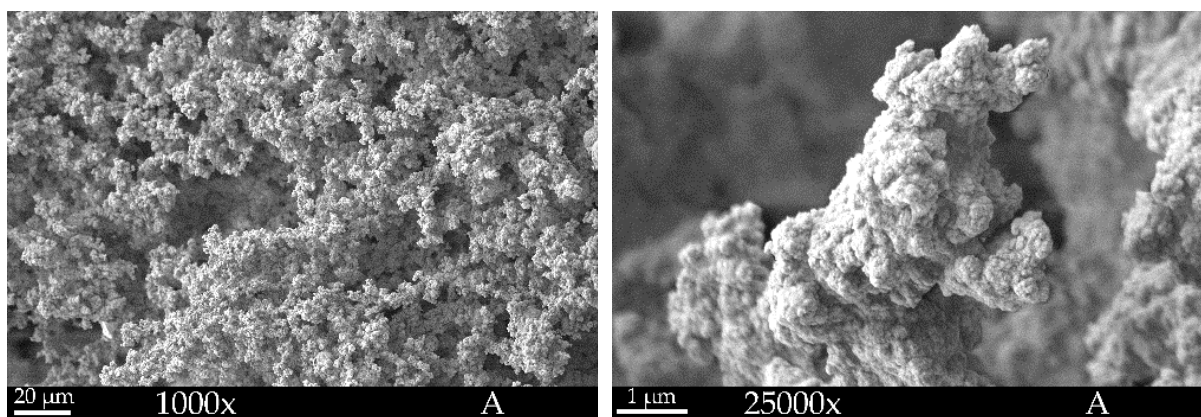

Figure 4.5 - SEM micrographs for sample A at 1000x and 25000x.

For sample A, in Figure 4.5, we can visualize a porous morphology with a random organization. This sample also seems to be constituted by the aggregation/linking of small structural units of very small dimensions ($\ll 1$ μm). At low magnification, it is noticeable that very large pores or regions without aerogel exist.
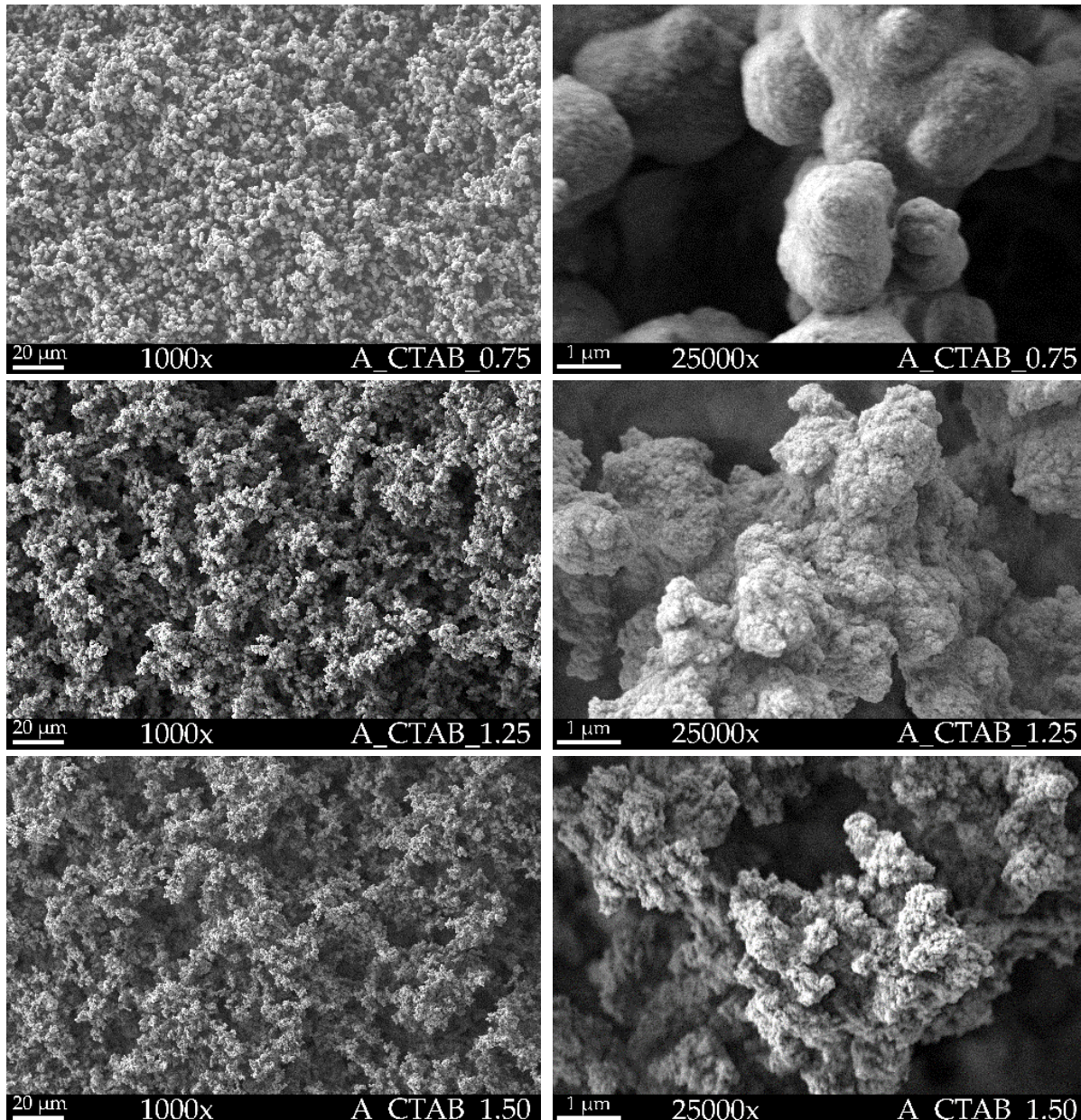
Figure 4.6 - SEM micrographs for samples A_CTAB_0.75, A_CTAB_1.25 and A_CTAB_1.50 at 1000x and 25000x.

By observation of A_CTAB_0.75 sample in Figure 4.6, it can easily be seen that the particles that constitute the structure are bigger, with distinct necks and the network does not exhibit large holes as in sample A. This is consistent with the previous results of a denser material. In samples A_CTAB_1.25 and A_CTAB_1.50 is seen that the presence of the surfactant is enough to create larger pores in the structure, but the network keeps a regular pattern. The particles that make up the nanostructure are once again much smaller than 1 μm. This is consistent with the reduction in the bulk density obtained for these samples.
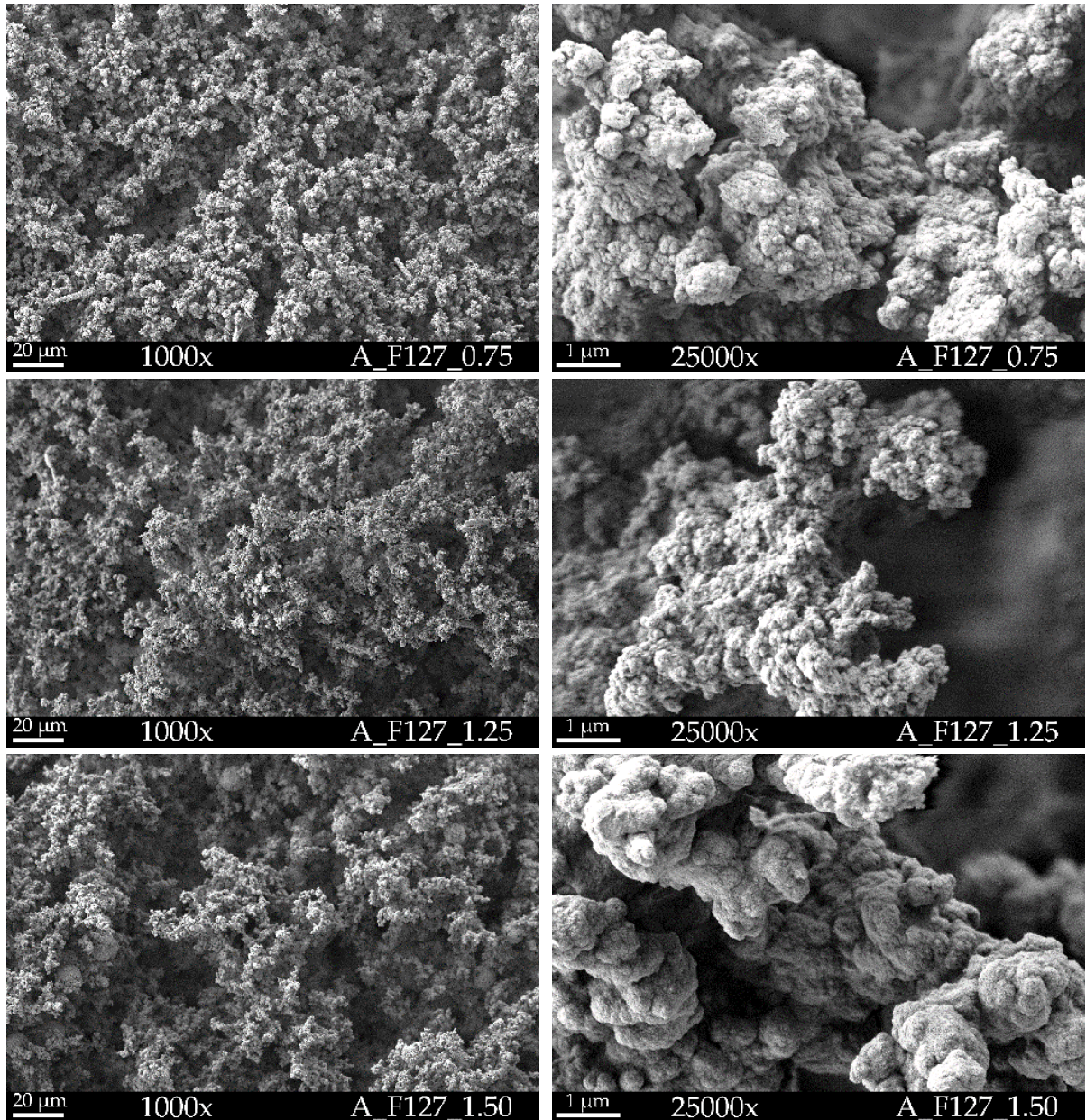
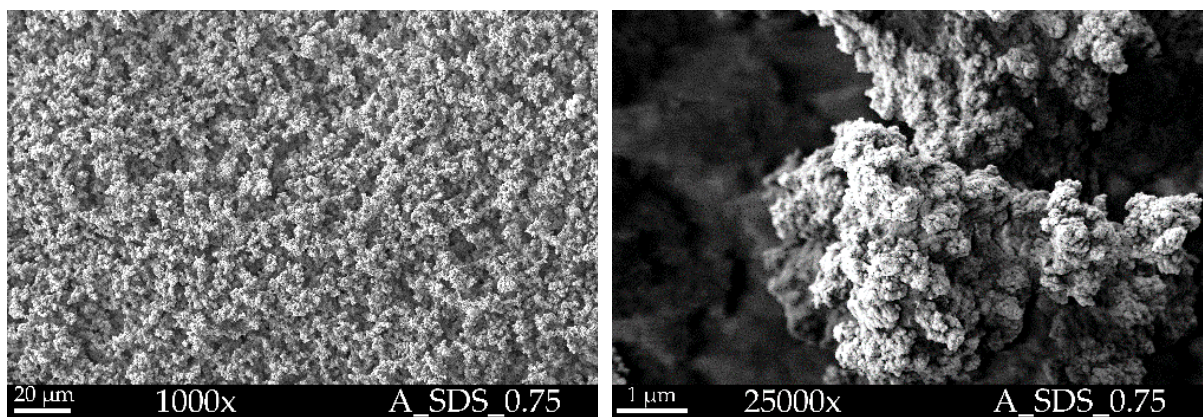Figure 4.7 - SEM micrographs for samples A_F127_0.75, A_F127_1.25 and A_F127_1.50 at 1000x and 25000x.

Figure 4.8 - SEM micrographs for sample A_SDS_0.75 at 1000x and 25000x.

Through the visualization of the micrographs in Figure 4.7 and in comparison with sample A, it can be said that in samples A_F127_0.75 and A_F127_1.25 the nanoparticles of the structure have a similar size to the ones in sample A but in sample A_F127_1.50 these nanoparticles seem to have grown and are more agglomerated. In general, in these micrographs the pores seem to be bigger than the ones in sample A, appearing again some large holes especially in sample A_F127_1.50. This is likely due to the fact that the F127 is a big molecule, with approximately 12600 Da, and it imprints huge holes in the structure when it is removed from there. It is also noticeable the presence, in all the micrographs of Figure 4.7, of some weird structures, in form of long rods and spheres, in the middle of the nanostructure. Possibly these are due to the achievement of the critical micellar concentration of the surfactant and the growth of the silica network inside the micelles (see the shape of micelles in section 2.4). The aforementioned structures are better seen in Figure 4.9.
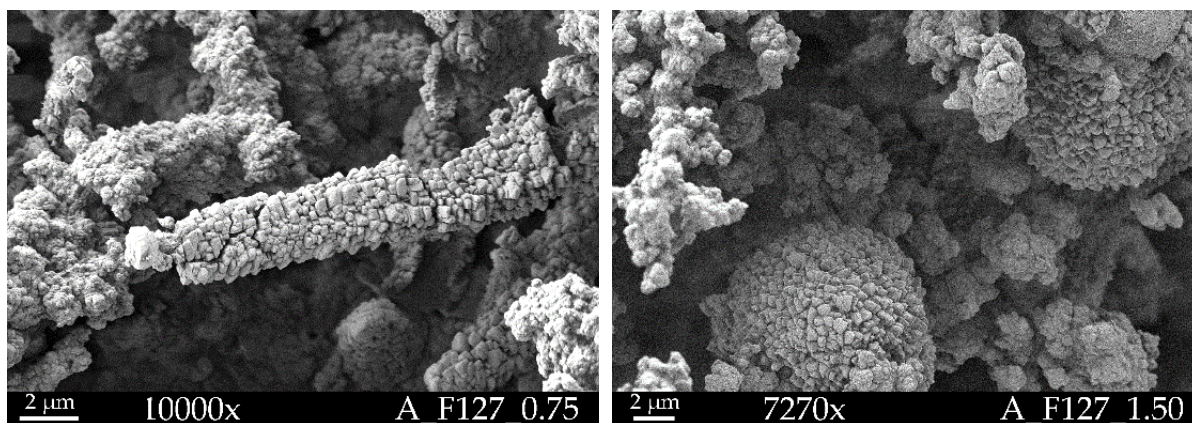
Figure 4.9 - SEM micrographs of the wierd structures produced when using F127.

When assessing Figure 4.8, we can immediately see the stark difference of the overall morphology of the sample A_SDS_0.75 when compared with sample A. The network is very dense and closed, with a homogeneous surface, unlike sample A. This sample clearly seems to have a much more regular nanostructure. Also mentionable is the size of the nanoparticles that is even much smaller than those in sample A. It is worth noting that these structural units, seen in all the micrographs of this section, are what is designated in the literature as secondary silica particles.

In summary, the SEM results seem to be consistent with the previously discussed topics, especially the fact that the charged surfactants should be the best to be used when wanting to synthesize a more organized silica structure.

4.3.3 ASAP

With the ASAP technique, it is now possible to ascertain properties like specific surface area and the average pore size distribution of the materials, which can validate (or not) the conclusions drawn until this point.

The evaluation of the results will be conducted in three stages. The first stage presents the specific surface area, in Table 4.6, and the respective reached correlation by application of the BET theory; the second is where the equations of Kelvin and Halsey are applied through the BJH's algorithm, giving the results presented in Table 4.7; and in the third stage, Figure 4.10 shows the obtained desorption results for the pore size distribution.

Table 4.6 - Specific surface area of the selected aerogels.

Sample	A_s BET (m²/g)	R^2
A	321.8 ± 6.5	0.9992
A_CTAB_1.25	435.7 ± 7.1	0.9995
A_F127_1.25	181.0 ± 9.2	0.9949
A_SDS_0.75	345.2 ± 5.9	0.9994

By observation of Table 4.6, it can be concluded that the sample with the highest specific surface area is sample A_CTAB_1.25, which is consistent with the previous assumption that this would be the ideal type and amount of surfactant to be used in order to improve the base properties of a MTMS-derived aerogel synthesized under the established conditions. The sample A_F127_1.25 presents the lowest specific surface area, again in agreement with the obtained SEM and density results. The surface area is lower than that obtained for sample A, possibly because the polymer F127 leads to the closing of part of the pores. It should be also mentioned that, although sample A_SDS_0.75 has a higher specific surface area than sample A, there is not a significant difference between them, which was not expected since the previously obtained results indicate that A_SDS_0.75 could have a higher specific surface area.

Table 4.7 - Size and average pore volume for the selected aerogels.

Sample	BJH Desorption		BJH Adsorption	
	V_{pores} (cm³.g⁻¹)	$D_{average,\ pores}$ (Å)	V_{pores} (cm³.g⁻¹)	$D_{average,\ pores}$ (Å)
A	0.21	38.8	0.17	46.7
A_CTAB_1.25	0.20	37.2	0.14	45.7
A_F127_1.25	0.09	40.2	0.09	37.8
A_SDS_0.75	0.21	51.7	0.14	49.9

In Table 4.7, the visible results demonstrate that the samples A_F127 and A_SDS_0.75 desorbed more than what they adsorbed, meaning that there was gas still trapped inside the

pores and the previous degasification of the material was not sufficient. The pores volume was similar between samples A, A_CTAB_1.25 and A_SDS_0.75 in the desorption or adsorption regimes. However, the results for sample A_F127_1.25 present a pore volume that is half of the other samples, which is lower than the expected for this sample, considering the differences in Figure 4.5 and 4.7. Table 4.7 also reveals that the biggest average pore diameter corresponds to sample A_SDS_0.75, in agreement with the previous obtained results, because with the same volume of pores as in samples A and A_CTAB_1.25 the specific surface area is lower than the one in A_CTAB_1.25. Also mentionable is the fact that the results for A_CTAB_1.25 are also consistent, since, with higher specific surface area and similar pores volume between samples, the average pore diameter had to be at least lower than the pore diameter of sample A. As for the sample A_F127_1.25, the results obtained in Table 4.7 are coherent with the drop in specific surface area, because even if the average pore diameter is similar, there are fewer pores for this sample.

From Table 4.7 it is noticeable that the average pore diameter is predominantly between 3.7 and 5.2 nm, in the range of mesopores (2 nm < mesopores < 50 nm) which is further confirmed in Figure 4.10, where the pore size distributions are shown. It should be mentioned that this technique cannot effectively measure pores below 2 nm (micropores) or much larger than 100-200 nm, meaning that the average pore diameter may not represent well the real value.
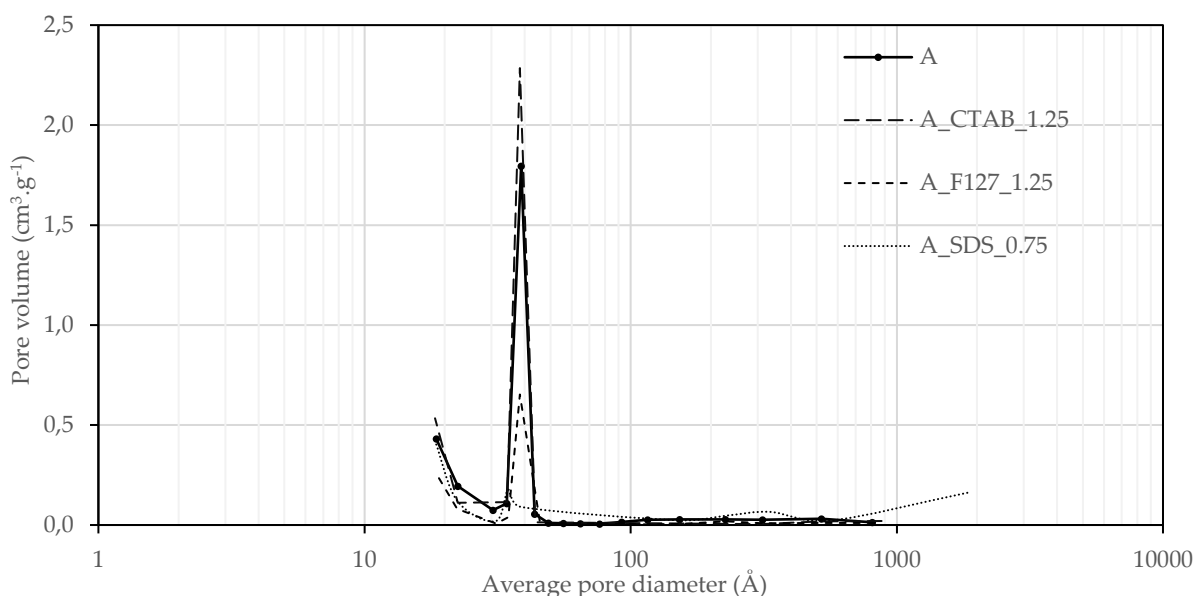
Figure 4.10 - Pore size distribution for the analyzed materials.

Figure 4.10 proves that the average pore diameter is in fact in the mesopores range, with exception of the A_SDS_0.75 sample that indicates the absence of mesopores. This is consistent with discussion in subsection 4.2.4 (zeta potential results), where is stated that there may be repulsion between the MTMS-derived particles and the SDS heads. This can lead to higher aggregation of the silica secondary particles (between themselves), leading to higher extent of

condensation and filling of mesoscale pores. On the other hand, there is an increase in the pore volume in the range or pores higher than 100 nm, resulting in a higher average pore size (Table 4.7)

By observation of the individual results for adsorption and desorption isotherms in Appendix E, it can be concluded that the obtained isotherms are of type IV [41][44], which is in agreement with the obtained average pore size. In fact, these type IV isotherms are characteristic of mesoporous solids, presenting an initial knee zone which represents the adsorption to a monolayer and also a cycle of hysteresis between the adsorption and desorption isotherms. According to the IUPAC classification, the obtained hysteresis cycle appears to be from type H4, typical of dead-end conical pores or of complex ramified geometries.

4.4 Mechanical characterization of the aerogels

The stress-strain diagrams for the selected samples are presented in Figure 4.11. None of the test samples broke during the test. The calculated Young's moduli for these samples are presented in Table 4.8, for several parts of the stress-strain curve.
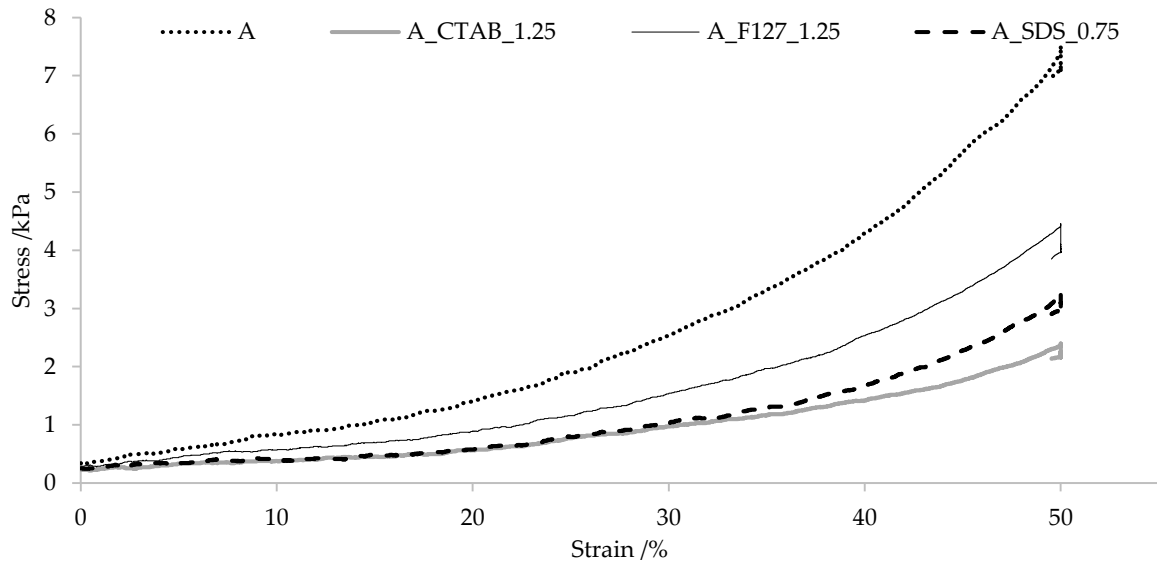
Figure 4.11 - Stress-strain diagram obtained up to 50 % compression of the samples.

Table 4.8 - Young's modulus for the selected samples.

Sample	$E_{0\ to\ 15\%}$ **(kPa)**	R^2	$E_{15\ to\ 25\%}$ **(kPa)**	R^2	$E_{15\ to\ 30\%}$ **(kPa)**	R^2
A	4.7	0.994	8.5	0.988	9.9	0.985
A_CTAB_1.25	1.5	0.966	3.0	0.968	3.6	0.982
A_F127_1.25	2.7	0.977	4.8	0.986	5.6	0.986
A_SDS_0.75	1.2	0.887	3.2	0.966	3.9	0.978

All samples have similar stress-strain curves, characteristic of viscoelastic materials. Sample A is the most rigid sample, confirmed by the higher value of the Young's modulus (Table 4.8). The surfactants increased flexibility of the aerogels, shown by the reduction of the value of Young's moduli. This tendency was observed when handling the samples and is consistent with the lower bulk density obtained for the samples with surfactant. The increased flexibility was most significant with 1.25 g of CTAB that featured a modulus of approximately a third of sample A. This cationic surfactant seems to be the one leading to most promising properties of the monoliths, which is consistent with a strong interaction of the surfactant positive head with the negative charge of the aerogels (as observed by zeta potential). As it can be observed, the Young's modulus increases depending on the strain already achieved in the sample (region where the linear regression is applied), since when the sample is under a higher strain (*i.e.*, with more effective bulk density), more resistance it will oppose to further deformation. This is typical of viscoelastic materials because they have the ability to absorb and accommodate the load that is applied to them, but after removing the load they return to the initial shape/size [45]. The deformation during this process is mainly accommodated by the reduction of the size of larger pores originating a flow of the air inside them.

4.5   Results of the simulated systems

Recalling what was previously said in subsections 2.5.2 and 3.3.5 on the most likely cluster conformations formed by MTMS, the cyclic conformation with 4 silicon atoms (hereafter called SI4) and the cage-like conformation with 8 silicon atoms (SI8) were studied. Both SI4 and SI8 were simulated in various quantities, labelled as B1, B2 and B3 for SI4 and C1, C2 and C3 for SI8, and the numbering means that B1 and C1 have both 360 Si atoms, B2 and C2 have 320, and B3 and C3 have 280.

4.5.1   VMD

The VMD tool was used to obtain the snapshots presented in Figures 4.12 to 4.14. Figure 4.12 presents the simulation boxes at t=0 ns, in which only the MTMS-derived particles, SI4 (simulation B1) and SI8 (simulation C1), are represented (the other specimens included in the simulations, viz. methanol and CTAB, are not shown for the sake of simplicity; all the figures have pictures in the same orthographic frontal view as seen by the axis displayed in each picture and for better understanding of the evolution of the simulations please consult Appendix F). The algorithm randomly places the particles inside the simulation box, and these data are enough to establish a base point for comparison with the pattern reached at the end of the simulation (t=80 ns) as shown in Figures 4.13 and 4.14.
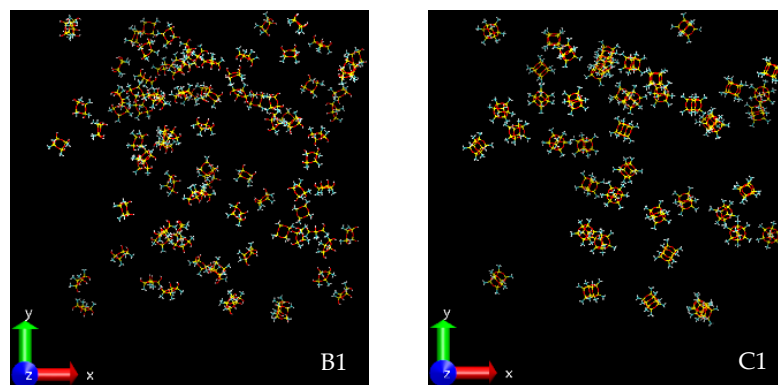
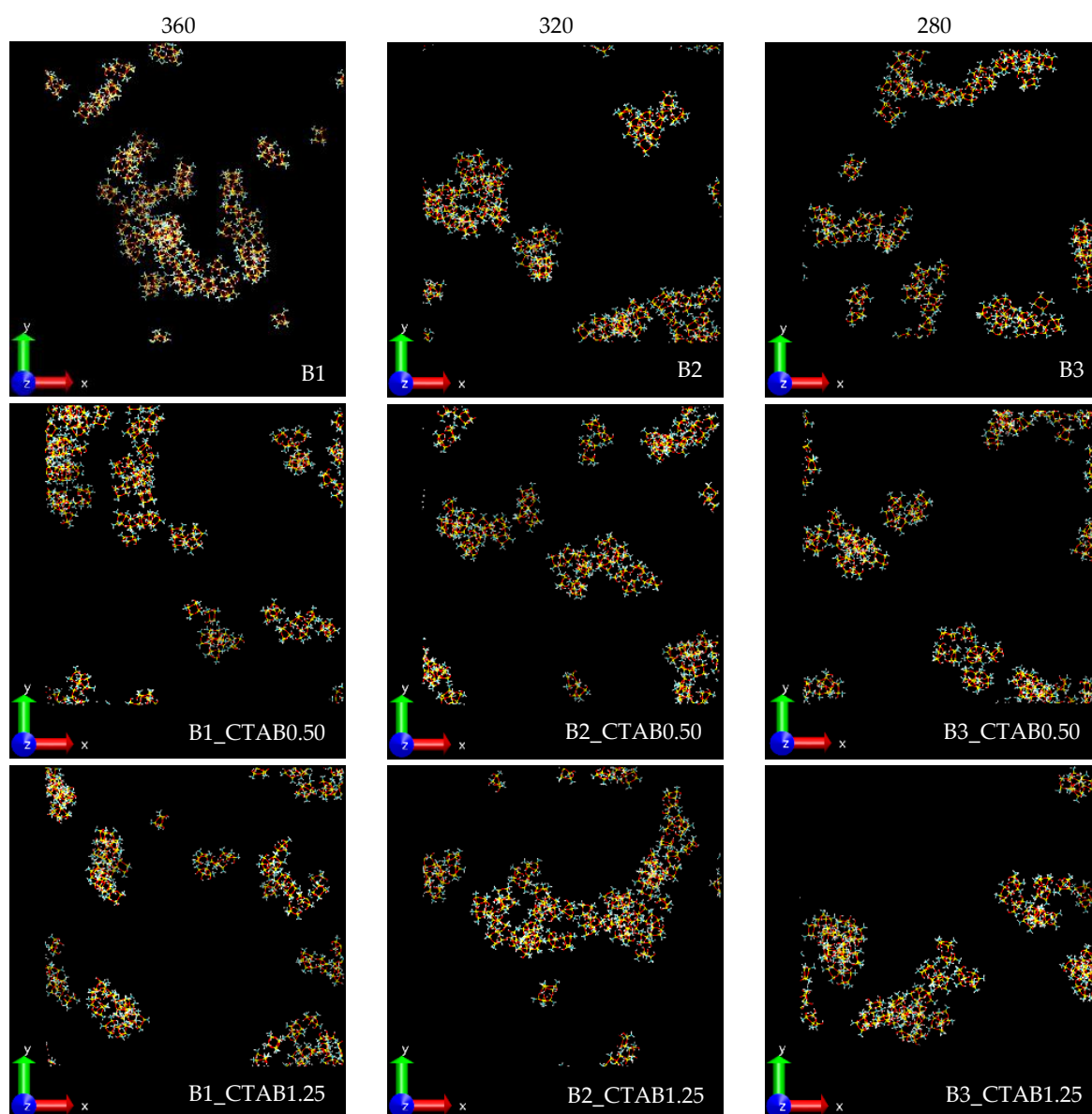Figure 4.12 - Simulation boxes at *t*=0 for B1 and C1 (see text for labeling).

Figure 4.13 - Simulation boxes after *t*=80 ns for the indicated for MTMS-derived SI4, with and without surfactant (see text for labeling).
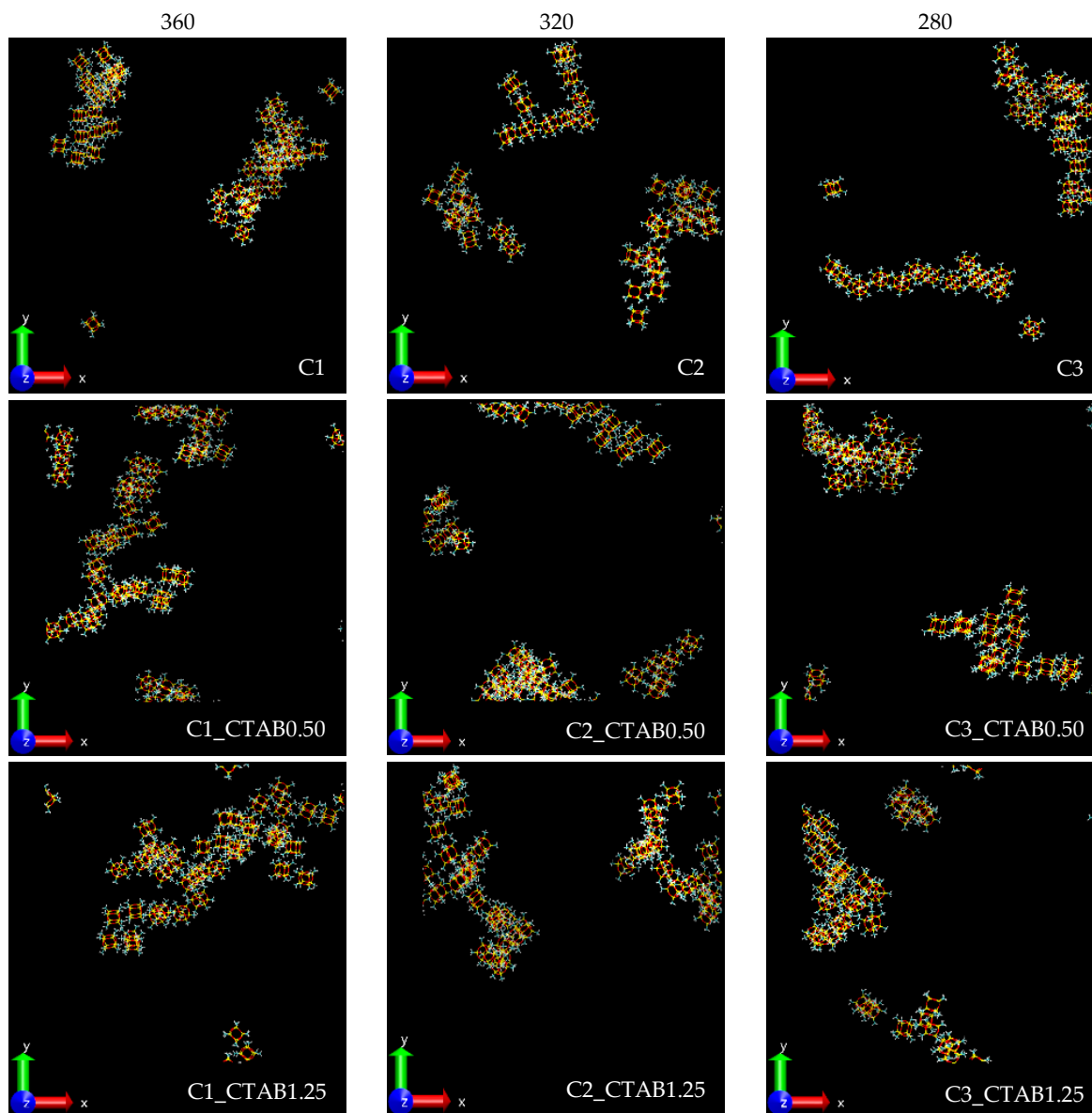
Figure 4.14 - Simulation boxes after *t*=80 ns for the indicated for MTMS-derived SI8, with and without surfactant (see text for labeling).

It can be easily seen from Figure 4.12 that in any case the particles start out dispersed in the simulation box. On the other hand, when looking at Figure 4.13 and Figure 4.14, it is clear that both SI4 and SI8 specimens tend to form aggregates or clusters, which is consistent with information known from experimental grounds. Although different amounts of surfactant were used, it is not possible to ascertain just by looking at the snapshots whether such a variable influences the number of entities present in the former clusters. However, it is possible to say that the final structures are different in every scenario. Furthermore, the structures formed from SI4 seem to be more compact, which can be explained, apart differences in the molecular volume (lower in SI4 than in SI8), by the contribution of hydrogen bonding, possible in SI4 but not in the caged structures.

4.5.2   hbond

This subsection summarizes the results related to hydrogen bond formation between the Si based particles, applicable only to the SI4 specimen, with the trajectories of interest being presented in Figure 4.15 and 4.16.
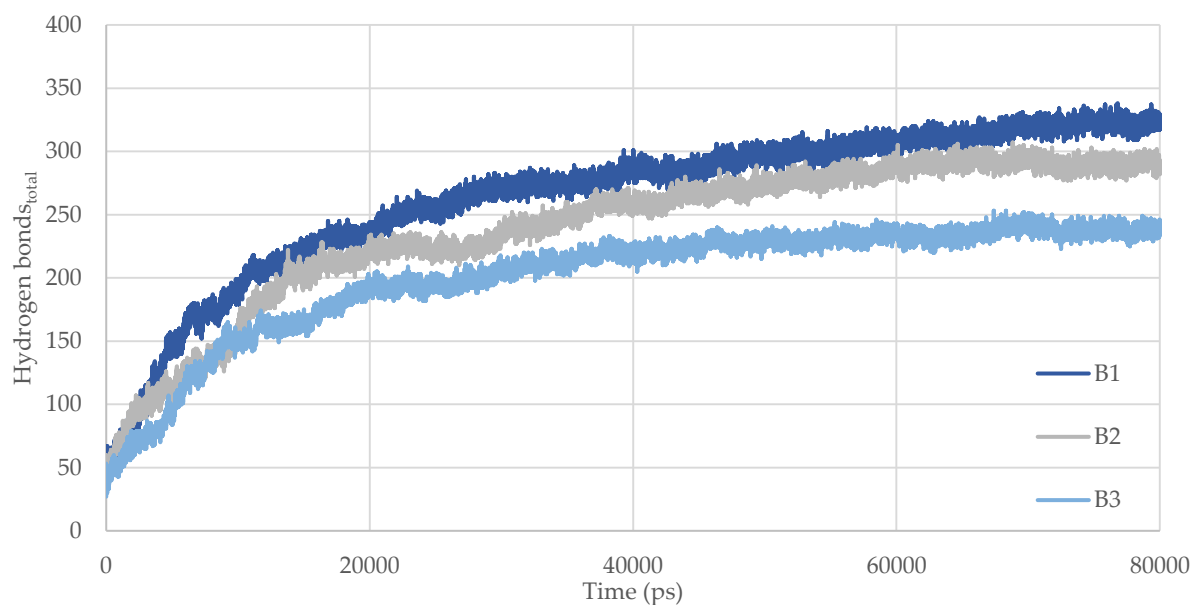

Figure 4.15 - Total number of hydrogen bonds between SI4 moieties, without surfactant, as a function of time, in the indicated simulations (see text labelling).
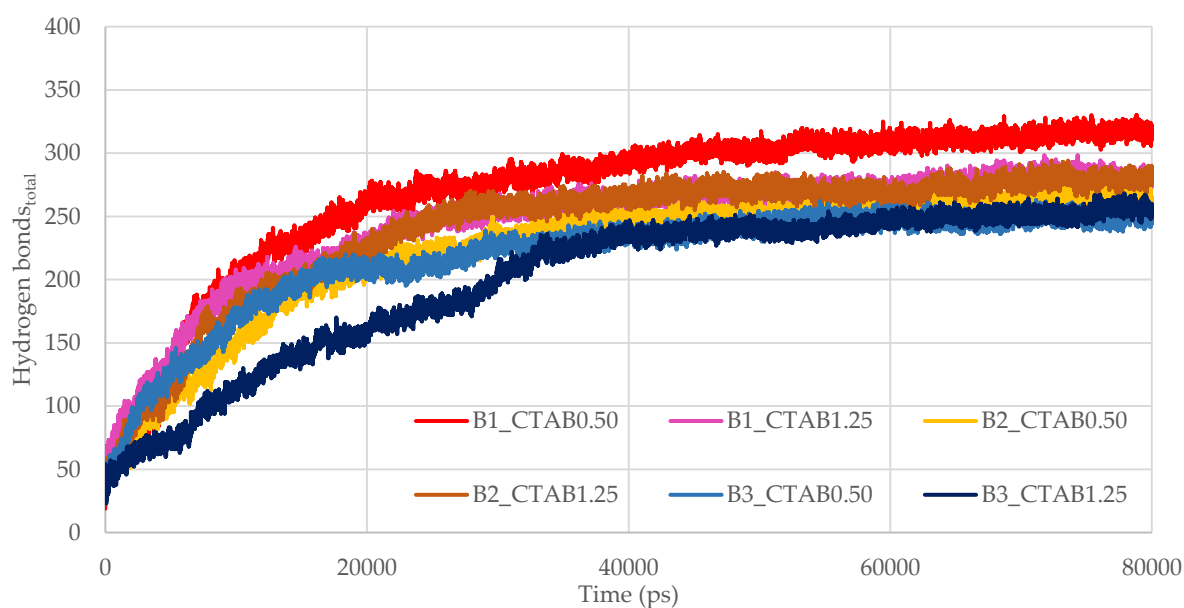

Figure 4.16 - Total number of possible hydrogen bonds between SI4 moieties, with surfactant, as a function of time, in the indicated simulations (see text for labeling).

Looking at Figure 4.15 it is observed that number of hydrogen bonds formed increases with the simulation time and with the concentration of Si4. This is an expected result because the more SI4 in a fixed volume, the more likely is their interaction through hydrogen bonding. In fact, the hydroxyl groups present in SI4 (and absent in SI8) should contribute to the MTMS-derived aerogels structure growing, leading to the condensation reactions presented in subsection 2.3.1.

The results in Figure 4.16 show that the presence of CTAB in the system leads to an increase in the rate of the hydrogen bonds at the early simulation stage, the B3_CTAB1.25 being the only exception. In the B3 simulations the presence of CTAB at the end of 80 ns seems to not affect the number of possible hydrogen bonds. As for the B2 simulations some apparent effect is noted because the simulation without surfactant in Figure 4.15 stabilizes close to 300 hydrogen bonds, while with CTAB shown in Figure 4.16 are both closer to 275. No noticeable differences are found between B1 and B1_CTAB0.50 cases. However, the simulation for the optimal laboratory bulk density, B1_CTAB1.25, presents a similar result after 80 ns as the simulation B2 in Figure 4.15. This means that more particles would be necessary to better assess the actual effect of the surfactant in the of hydrogen bonds formation.

4.5.3   clustsize

The analysis of the clusters formed can be done from the results in Figures 4.17 to 4.19, which show the number of free MTMS-derived particles, SI4 and SI8, and from the results that show the maximum size of clusters in Figures 4.20 to 4.22.

Free MTMS-derived particles in the simulation
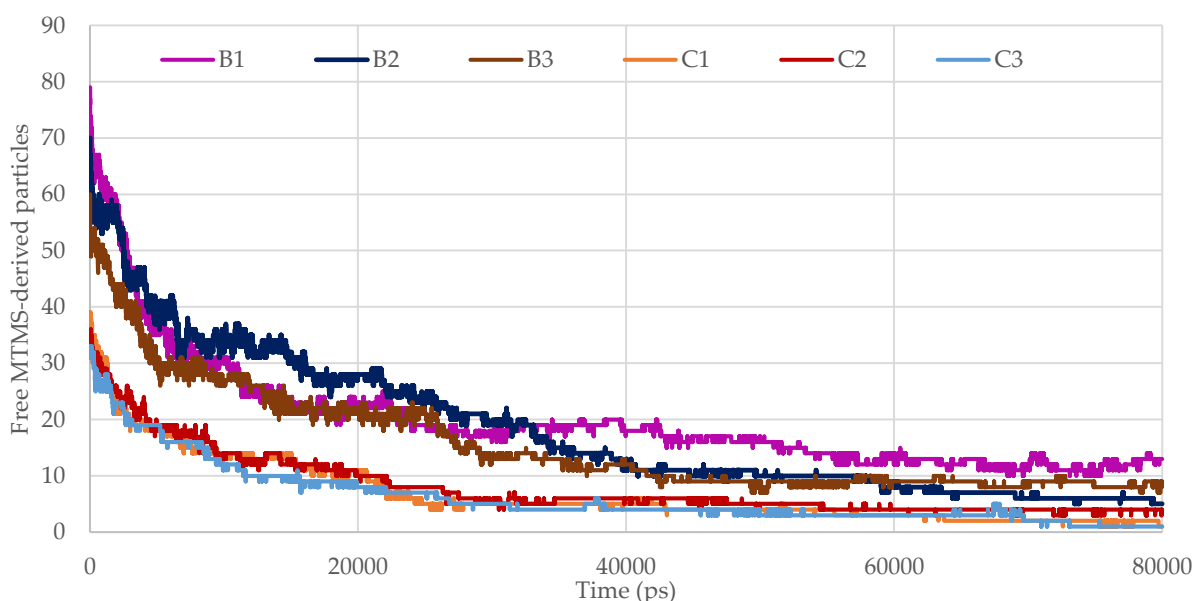
Figure 4.17 - Number of free MTMS-derived SI4, without surfactant, as a function of time (see text for labeling).
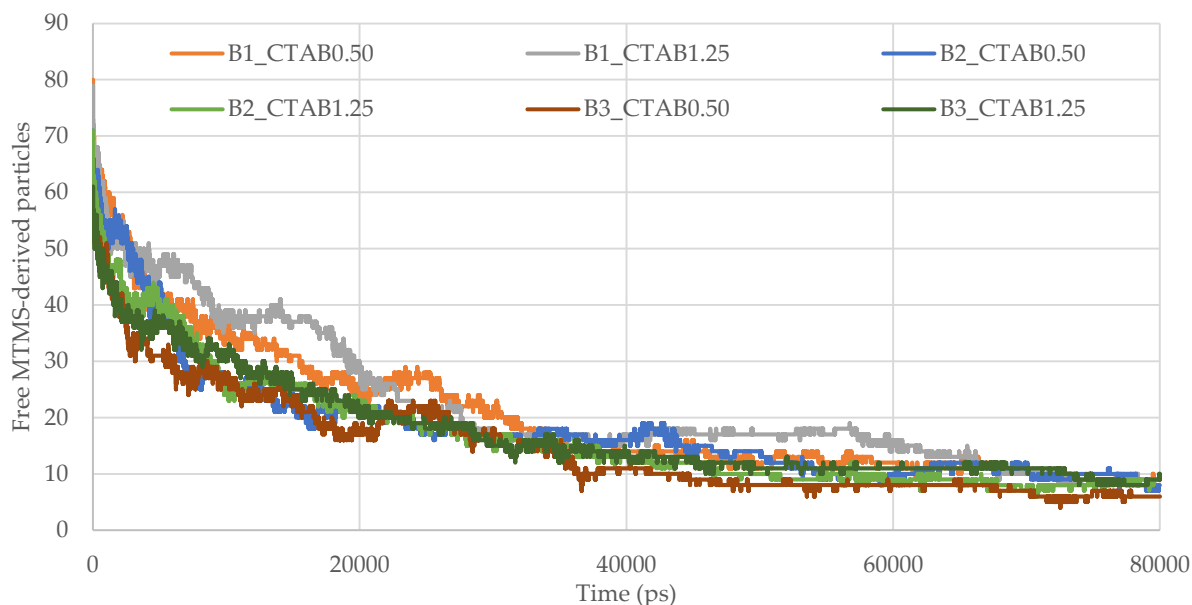
Figure 4.18 - Number of free MTMS-derived SI4, with surfactant, as a function of time (see text for labeling).
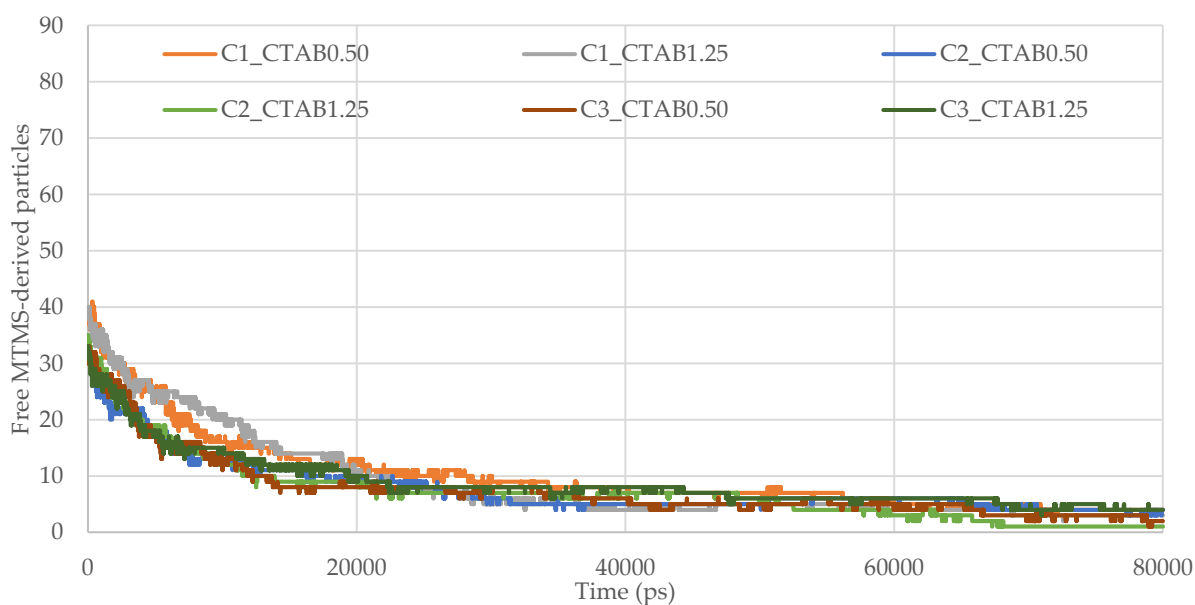
Figure 4.19 - Number of free MTMS-derived SI8, with surfactant, as a function of time (see text for labeling).

The results in Figure 4.17 quantitatively confirm the formation of clusters previously seen in subsection 4.5.1 (VMD). Both the simulations with SI4 (B1, B2 and B3) and with SI8 (C1, C2 and C3) tend to have fewer free particles at t=80 ns when compared to those at the very beginning of the simulations. The pattern is the same whatever the number of MTMS-derived particles considered, although the C1, C2 and C3 series (SI8 based systems) appear to be less sensible to that variable.

Analyzing the results in both Figure 4.18 and 4.19 no significant changes in the trajectory profiles are found when compared to those in Figure 4.17. This metric does not allow to clearly capture the influence, if any, of the surfactant in the cluster formation.

Maximum size of clusters

Figure 4.20 - Maximum size of clusters(in terms of molecule number), without surfactant, as a function of time(see text for labeling).

The results in Figure 4.20 indicate that the number of MTMS-derived particles initially inserted in the 10 nm^3 box does not appear to be a factor in the maximum size of the clusters formed. No clear trends can be drawn for the simulated systems from this metric.
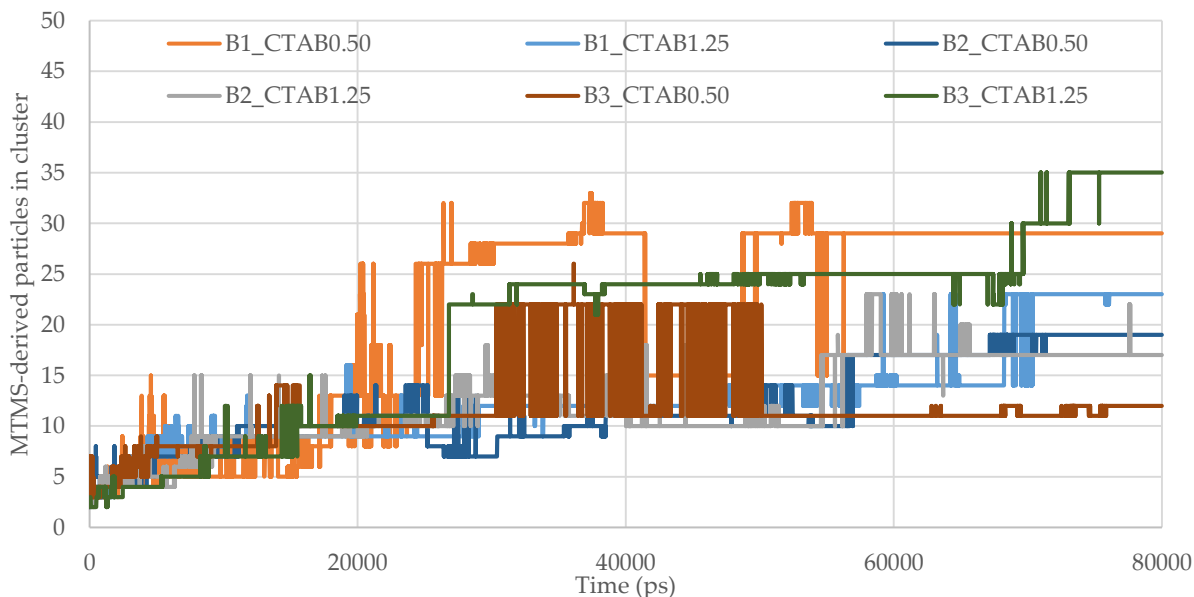
Figure 4.21 - Maximum size of clusters(in terms of molecule number) for SI4 particles, with surfactant, as a function of time (see text for labeling).

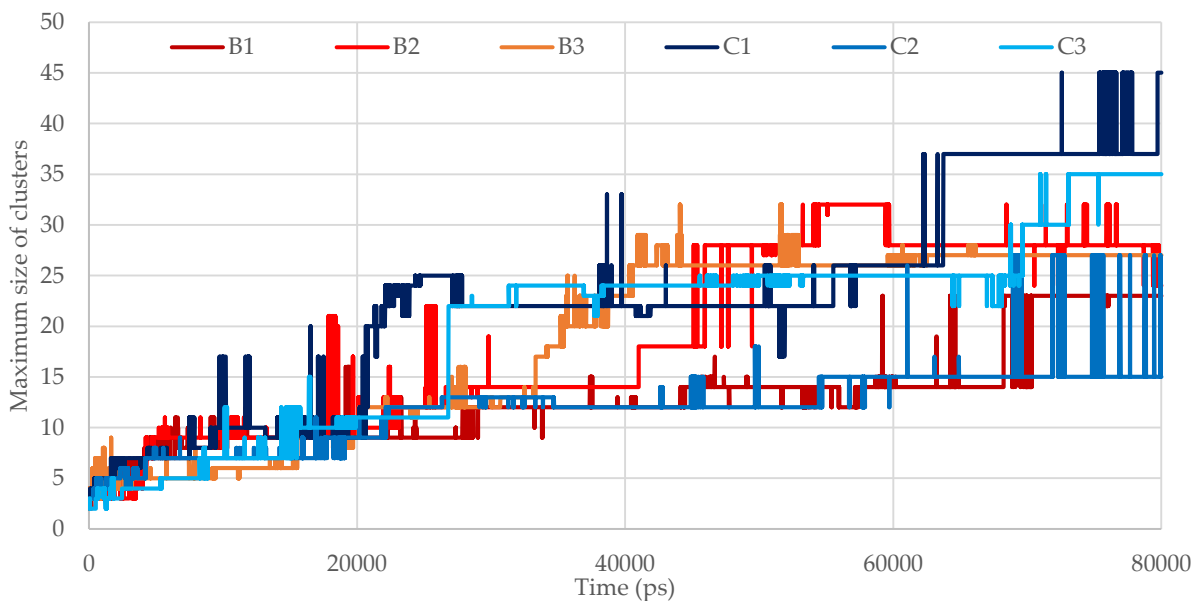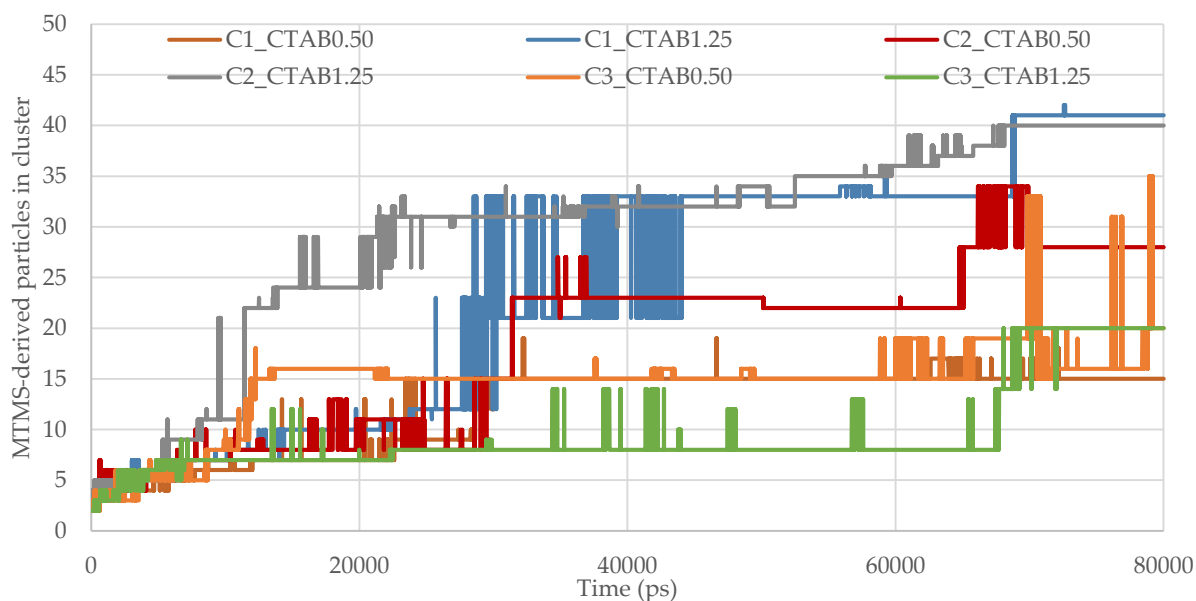Figure 4.22 - Maximum size of clusters(in terms of molecule number) for SI8 particles, with surfactant, as a function of time (see text for labeling).

Overall, the results in Figures 4.21 and 4.22 suggest that the presence of the surfactant seems to reduce the maximum size of a cluster made by MTMS-derived particles. Like as experimentally observed, the presence of the surfactant in the molecular dynamics results shows differences in the end results although no real parallelism was able to be established.

It should be stressed that a simulation time of the 80 ns might be not enough to describe the experimental conditions. Furthermore, a model which, besides the solvent and surfactant, includes a single SI4 or SI8 specimen is certainly an oversimplification of the reality. It should be realized, however, that this computational study is nothing but a first step of an expected comprehensive approach, in which a combination of various MTMS-derivatives and larger simulation times must be considered.

5   Conclusions and future prospects

In this work, the effect of different types of surfactants on the microstructure of silica based aerogels derived from MTMS was studied. The surfactants chosen for this work represent several kinds: SDS as anionic, CTAB as the cationic and F127 as non-ionic. Different amounts of surfactant were added to the gel synthesis and these were conditioned by the supercritical drying step, going from 0.50 g to 1.50 g with the CTAB and F127, and from 0.50 g to 0.75 g with SDS.

The synthesized materials were characterized chemically, physically/structurally and mechanically. These results allowed to ascertain the effects of the surfactants in the sol-gel chemistry and final material properties.

The most promising aerogels were chosen based on the bulk density and the observable characteristics. The envisaged aerogels have lower bulk density, higher flexibility and should feature low particle shedding. Considering this, the selected samples were A, A_CTAB_1.25, A_F127_1.25 and A_SDS_0.75, where sample A is the sample without surfactant that serves as a base comparing point and, in the others, surfactants were used in the synthesis with the indicated amounts (in g).

From the chemical analysis, it was concluded that the aerogels are made up of a silica matrix with methyl groups, consistent with the structure expected from the MTMS precursor. Also, there is evidence that residual amounts of surfactant are still present in the final structure, due to the difference in % C between the pure sample and the samples with surfactant. The contact angle assessment revealed that the starting material is already quite hydrophobic (θ_c = 136°), however, surfactants tend to increase this characteristic (up to 149°). Moreover, the zeta potential showed that the MTMS-derived particles are negatively charged (-9.25 mV) in their surface, meaning that the cationic surfactant, CTAB, interacts electrostatically with the MTMS-derived aerogel.

From a structural point of view, it was found that the use of surfactants does not hinders the highly porous nature of the aerogels. The specific surface area of the materials was impacted by the type of surfactant used: CTAB increased this property while F127 lowered it ($A_{s,\ CTAB}$ = 436; $A_{s,\ F127}$ = 181; $A_{s,\ SDS}$ = 345; $A_{s,\ puro}$ = 322 $m^2.g^{-1}$).

The SEM analysis reveals a microstructure consistent with organically modified silica aerogels. This result is in agreement with the FTIR analysis that revealed the formation of the MTMS-derived matrix. The amount and type of surfactant added originated different microstructures in terms of particle shape and sizes and pore sizes.

As it was already noticeable by the handling of the samples, the surfactants decreased the value of the Young's modulus (which was already extremely low, < 9.9 kPa), increasing the flexibility of these materials by up to four times (comparing the modulus obtained with a strain from 0 to 15%). The obtained aerogels are extremely flexible not breaking with compressions up to 50 % strain. CTAB was the surfactant which led to the most flexible aerogels.

Within the framework of molecular dynamics based study, two types of MTMS derived specimens were considered: one cyclic, with 4 silicon atoms (SI4), and the other, a cage-type molecule with 8 silicon atoms (SI8). By varying the total number of silicon atoms from Si8 and Si4 specimens and CTAB in the simulation box, the trajectories of 80 ns simulations were analyzed. Being an exploratory study, the results obtained from this approach were not conclusive, possibly because the simulation time was not long enough to appropriately study these systems. Nonetheless, the simulations showed that hydrogen bonds are formed and the initial MTMS derivatives are prone to aggregate into clusters. The structures formed from SI4 seem to be more compact, which can be explained, apart the differences in the molecular volume (lower in SI4 than in SI8), by the contribution of hydrogen bonding. The presence of CTAB seems to affect the clusters, diminishing their sizes.

The computational work was restricted by the computational resources. Different simulations should be performed including the variation of pH, the use of other MTMS based structures and mixtures thereof (the used specimens studied are a limited representation of reality). Better parameterized force fields and increased simulation time ought to improve the obtained results. Different metrics should also be employed to analyze the final results. Due to time constraints, it was not possible to study by molecular dynamics simulations the surfactants SDS and F127, used experimentally in this work. This task should be considered for future works.

As stated previously, for the proposed application of employing the synthesized aerogels for insulation in spatial applications and building construction, lightweight, porous and flexible materials are of utmost importance. As it can be seen, the aerogels prepared in this work contribute to the advance of these materials, as they show improved properties.

This dissertation extensively studied the effects of various surfactants in the MTMS sol-gel system for given molar ratios of the reactants. Because the used surfactants were not studied before with this system, new optimization of the ratios of the reactants may be necessary and should be considered for future works. Also new surfactants could be studied, testing the remaining types of surfactants and other cationic surfactants. Other properties, like insulation properties and more mechanical tests should be performed to further characterize the obtained materials.

References

1. M. A. Aegerter, N. Leventis, M. M. Koebel, (Eds.), *Aerogels Handbook* (*Advances in Sol-Gel Derived Materials and Technologies*), Springer, New York, 2011.

2. H. Maleki, L. Durães, A. Portugal, An overview on silica aerogels synthesis and different mechanical reinforcing strategies, *Journal of Non-Crystalline Solids*, 385 (2014) 55-74.

3. J. L. Gurav, I.-K. Jung, H.-H. Park, E. S. Kang, D. Y. Nadargi, Silica Aerogel: Synthesis and Applications, *Journal of Nanomaterials*, 2010 (2010) 1-11.

4. A. S. Dorcheh, M. H. Abbasi, Silica aerogel; synthesis, properties and characterization, *Journal of Materials Processing Technology*, 199 (2008) 10-26.

5. L. Durães, M. Ochoa, A. Portugal, N. Duarte, J. P. Dias, N. Rocha, J. Hernandez, Tailored Silica Based Xerogels and Aerogels for Insulation in Space Environments, *Advances in Science and Technology*, 63 (2010) 41-46.

6. L. Durães, M. Ochoa, N. Rocha, R. Patrício, N. Duarte, V. Redondo, A. Portugal, Effect of the Drying Conditions on the Microstructure of Silica Based Xerogels and Aerogels, *Journal of Nanoscience and Nanotechnology*, 12 (2012) 6828-6834.

7. L. Durães, A. Maia, A. Portugal, Effect of additives on the properties of silica based aerogels synthesized from methyltrimethoxysilane (MTMS), *The Journal of Supercritical Fluids*, 106 (2015) 85-92.

8. *Encyclopædia Britannica*, in: http://www.britannica.com/science/gel, retrieved 17-06-2016.

9. *Encyclopædia Britannica*, in: http://www.britannica.com/science/sol-colloid, retrieved 17-06-2016.

10. Ryan Maloney, *Solgel 1*, in: https://www.youtube.com/watch?v=VlWGIKCV_6k, retrieved 27-05-2016.

11. L. Durães, T. Matias. R. Patrício, A. Portugal, Silica based aerogel-like materials obtained by quick microwave drying, *Mat.-wiss. u. Werkstofftech*, 44(5) (2013) 380-385.

12. R. A. Strøm, Y. Masmoudi, A. Rigacci, G. Petermann, L. Gullberg, B. Chevalier, M.-A. Einarsrud, Strengthening and aging of wet silica gels for up-scalling of aerogel preparation, *J Sol-Gel Sci Techn*, 41 (2007) 491-298.

13. *Silica Aerogel*, in: http://www.aerogel.org/?p=345 (2008), retrieved 31-07-2016.

14. Richard Farn (Ed.), *Chemistry and Technology of Surfactants*, Blackwell Publishinng Ltd, 2006.

15. Y. Wan, D. Zhao, On the Controllable Soft-Templating Approach to Mesoporous Silicates, *American Chemical Society*, 107 (2007) 2821-2860.

16. G. Hayase, K. Kanamori, M. Fukuchi, H. Kaji, K. Nakanishi, Facile Synthesis of Marshmallow-like Macroporous Gels Usable under Harsh Conditions for the Separation of Oil and Water, *Angew. Chem. Int. Ed.*, 52 (2013) 1-5.

17. G. Hayase, K. Kanamori, K. Nakanishi, Structure and properties of polymethylsilsesquioxane aerogels synthesized with surfactant n-hexadecyltrimethylammonium chloride, *Microporous and Mesoporous Materials*, 158 (2012) 247-252.

18. K. Kanamori, K. Nakanishi, T. Hanada, Sol-gel synthesis, porous structure, and mechanical property of polymethylsilsesquioxane aerogels, *Journal of Ceramic Society of Japan*, 112(12) (2009) 1333-1338.

19. K. Kanamori, G. Hayase, K. Nakanishi, T. Hanada, Pore Structure and Mechanical Properties of Poly(methylsilsesquioxane) Aerogels, *Materials Science and Engineering*, 18 (2011).

20. M. Kurahashi, K. Kanamori, K. Takeda, H. Kaji, K. Nakanishi, Role of block copolymer surfactant on the pore formation in methylsilsesquioxane aerogel systems, *The Royal Society of Chemistry*, 2 (2012) 7166-7173.

21. K. Kanamori, Y. Kodera, G. Hayase, K. Nakanishi, T. Hanada, Transition from transparent aerogels to hierarchically porous monoliths in polymethylsilsesquioxane sol-gel system, *Journal of Colloid and Interface Science*, 357 (2011) 336-344.

22. A. V. Rao, S. D. Bhagat, H. Hirashima, G. M. Pajonk, Synthesis of flexible silica aerogels using methyltrimethoxysilane (MTMS) precursor, *Journal of Colloid and Interface Science*, 300 (2006) 279-285.

23. A. V. Rao, M. M. Kulkarni, S. D. Bhagat, Transport of liquids using superhydrophobic aerogels, *Journal of Colloid and Interface Science*, 285 (2005) 413-418.

24. D. C. Young, *Computational Chemistry A Practical Guide for Applying Techniques to Real-World Problems*, John Wiley & Sons, 2001.

25. E. J. Maginn, J. R. Elliot, Historical Perspective and Current Outlook for Molecular Dynamics As a Chemical Engineering Tool, *Ind. Eng. Chem. Res.*, 49 (2010) 3059-3078.

26. C. J. Cramer, *Essentials of Computational Chemistry Theories and Models*, 2nd ed., John Wiley & Sons, Minnesota, 2004.

27. Abraham, M., Hess, B., van der Spoel, D., Lindahl, E., and the GROMACS development team, *GROMACS User Manual version 5.1.3*, in: www.gromacs.org, 2016.

28. Abraham, M., Hess, B., van der Spoel, D., Lindahl, E., and the GROMACS development team, in: http://www.gromacs.org/About_Gromacs, retrieved 25-07-2016.

29. Malde, A.K., Zuo, L., Breeze, M., Stroet M., Poger, D., Nair, P. C., Oostenbrink, C., Mark, A. E., An Automated force field Topology Builder (ATB) and repository: version 1.0., *Journal of Chemical Theory and Computation*, 7(12) (2011) 4026-4037.

30. GROMACS – flow chart, in: http://manual.gromacs.org/current/online/flow.html, retrieved 25-07-2016.

31. GROMACS – hbond, in: http://manual.gromacs.org/programs/gmx-hbond.html, retrieved 25-07-2016.

32. GROMACS – clustsize, in: http://manual.gromacs.org/programs/gmx-clustsize.html, retrieved 25-07-2016.

33. A. Borba, M. Almangano, A. A. Portugal, R. Patrício, P. N. Simões, Methylsilsesquioxane-Based Aerogel Systems – Insights into the Role of the Formation of Molecular Clusters, *The Journal of Physical Chemistry*, 120 (2016) 4079-4088.

34. E. V. Benvenutti, C. C. Moro, T. M. H. Costa, M. R. Gallas, Materiais híbridos à base de sílica obtidos pelo método sol-gel, *Quim. Nova*, 32(7) (2009) 1926-1933.

35. K. Kanamori, Monolithic silsesquioxane materials with well-defined pore structure, *J.Mater. Res.*, 29(23) (2014) 2773-1786.

36. J. Meneses, *Estudo do efeito das condições da etapa de catálise básica nas propriedades dos aerogéis obtidos a partir do precursor metiltrimetoxisilano (MTMS)*, Tese de Mestrado, Universidade de Coimbra, 2014.

37. L. G. Wade, *Organic Chemistry*, 8th ed., Pearson (2013).

38. B. J. Kirby, *Micro- and Nanoscale Fluid Mechanics: Transport in Microfluidic Devices*. Online ed. Cambridge University Press, in: http://www.kirbyresearch.com/index.cfm/wrap/textbook/microfluidicsnanofluidics.html, 2009.

39. J. A. A. Júnior, J. B. Baldo, The Behavior of Zeta Potential of Silica suspensions, *New Journal of Glass and Ceramics*, 4 (2014) 29-37.

40. T. Allen, *Particle Size Measurement – Surface area and pore size determination*, Vol. II, 5th ed., Kluwer Academic Publishers, 1999.

41. L. Durães, *Adsorção Física de Gases em Sólidos – medida de área de superfície específica e distribuição de tamanho de poros*, Notes from Caracterização Avançada de Materiais, Departamento de Engenharia Química da Universidade de Coimbra, Coimbra, 2012.

42. Y.-L. He, T. Xie, Advances of thermal conductivity models of nanoscale silica aerogel insulation material, *Applied Thermal Engineering*, 81 (2015) 28-50.

43. R. Al-Oweini, H. El-Rassy, Synthesis and characterization by FTIR spectroscopy of silica aerogels prepared using several $Si(OR)_4$ and $R''Si(OR')_3$ precursors, *Journal of Molecular Structure*, 919 (2009) 140-145.

44. A.P. Karnaukhov, *Adsorption: Texture of Dispersed and Porous Materials*, Novosibirsk: Nauka, 1999.

45. R. Lakes, *Viscoelastic Materials*, University of Wisconsin, in: http://silver.neep.wisc.edu/~lakes/VE.html, retrieved 06-09-2016.

Appendices

Appendix A – Xerogels previously synthesized with CTAB and F127

Table A.1 - Pictures and bulk densities with respective 95% confidence interval of the previously synthesized xerogels.

Sample	Photo	ρ_b (kg.m^{-3})
X		88.7 ± 16.4
X_F127_0.500		104.31
X_F127_0.250		90.8 ± 1.4
X_F127_0.100		90.8 ± 15.4
X_F127_0.050		91.8 ± 13.9
X_F127_0.025		86.3 ± 10.3
X_F127_0.010		81.5 ± 14.9
X_CTAB_1.000		84.6
X_CTAB_0.500		76.2

Table A.1 - Pictures and bulk densities with respective 95% confidence interval of the previously synthesized xerogels. (Cont.)

Sample	Photo	ρ_b (kg.m^{-3})
X_CTAB_0.250		89.23
X_CTAB_0.100		79.1 ± 5.1
X_CTAB_0.050		82.9 ± 27.2
X_CTAB_0.025		84.5 ± 15.3
X_CTAB_0.010		82.5 ± 12.1

Appendix B – Number of molecules/particles involved in simulations

- Calculations for the particles of each simulation.

Applying the molar ratio methanol/MTMS = 35, used in laboratory, and knowing that:

$$SI4 = 2 \times SI8$$

$$\text{Methanol}_{SI8} = 35 \times 8 \times SI8$$

$$\text{Methanol}_{SI4} = 35 \times 4 \times SI4$$

$$CTAB/MTMS_{\text{ratio}} = n_{\text{CTAB}}/n_{\text{MTMS}}$$

By defining the amount of SI8 it is possible to correlate all parameters and know how much molecules/particles are needed in each simulation box.

Table B.1 - Number of molecules/particles for each simulation.

Type of particle	Number of Particles	CTAB (g)	CTAB molecules	Methanol molecules	Total molecules/particles
SI8	45	---	---	12600	12645
	40	---	---	11200	11240
	35	---	---	9800	9835
SI8	45	0.50	20	12600	12665
		1.25	50		12695
SI8	40	0.50	18	11200	11258
		1.25	45		11285
SI8	35	0.50	16	9800	9851
		1.25	39		9874
SI4	90	---	---	12600	12690
	80	---	---	11200	11280
	70	---	---	9800	9870
SI4	90	0.50	20	12600	12710
		1.25	50		12740
SI4	80	0.50	18	11200	11298
		1.25	45		11325
SI4	70	0.50	16	9800	9886
		1.25	39		9909

Appendix C – Indexing the FTIR frequency vibrations

ν-stretching vibrations, $ν_s$-symmetric stretching vibration, $ν_{as}$-antisymmetric stretching vibration, $ν_β$-in-plane stretching vibration, δ-deformation vibration, $δ_s$-symmetric deformation vibration (bending), $δ_{as}$-antisymmetric deformation vibration (bending).

Table C.1 - Characteristic frequency vibrations and respective structural units for the MTMS-derived aerogels with CTAB.

Wavenumber (cm^{-1})					Vibration type	Structural unit
A_CTAB_0.50	A_CTAB_0.75	A_CTAB_1.00	A_CTAB_1.25	A_CTAB_1.50		
421	421	421	421	432	δ O-Si-O	-O-Si-O-
538	549	549	538	538	$ν_s$ Si-O	SiO$_2$ defects
676	676	676	676	676	$ν_s$ Si-O-Si	≡Si-O-Si≡
771	771	771	782	782	$ν_s$ Si-O	≡Si-O-Si≡
856	856	856	856	856	ν Si-C	Si-R
920	920	920	920	920	$ν_β$ Si-O	≡Si-OH
1026	1026	1026	1026	1026	$ν_{as}$ Si-O-Si	≡Si-O-Si≡
1121	1121	1121	1121	1121		
1270	1270	1270	1270	1270	$δ_s$ C-H	Si-R
1408	1408	1408	1408	1408	$δ_{as}$ C-H	Si-R
1620	1620	1631	1631	---	δ H-O-H	H-O-H
---	---	---	---	1737	$ν_s$ C=O	H$_2$C-CO-CH$_2$
2850	2850	2850	2861	2861	$ν_s$ C-H	-CH$_3$
2914	2914	2914	2925	2925	$ν_{as}$ C-H	-CH$_3$
2978	2978	2978	2978	2978	$ν_s$ C-H	-CH$_3$
3465	3465	3465	3465	---	OH and SiOH	H-O-H and ≡Si-OH

Table C.2 - Characteristic frequency vibrations and respective structural units for the MTMS-derived aerogels with F127.

Wavenumber (cm^{-1})					Vibration type	Structural unit
A_F127_0.50	A_F127_0.75	A_F127_1.00	A_F127_1.25	A_F127_1.50		
421	421	421	421	432	δ O-Si-O	-O-Si-O-
549	549	538	538	538	$ν_s$ Si-O	SiO$_2$ defects
676	676	676	676	676	$ν_s$ Si-O-Si	≡Si-O-Si≡
771	771	771	771	782	$ν_s$ Si-O	≡Si-O-Si≡
856	856	856	856	856	ν Si-C	Si-R
920	920	920	920	920	$ν_β$ Si-O	≡Si-OH
1026	1026	1026	1026	1026	$ν_{as}$ Si-O-Si	≡Si-O-Si≡
1121	1121	1121	1121	1121		
1270	1270	1270	1270	1270	$δ_s$ C-H	Si-R
1408	1387	1408	1408	1408	$δ_{as}$ C-H	Si-R
---	1620	1620	1620	1620	δ H-O-H	H-O-H
1737	---	---	---	---	$ν_s$ C=O	H$_2$C-CO-CH$_2$
2871	2850	2840	2840	2840	$ν_s$ C-H	-CH$_3$
2914	2914	2914	2925	2914	$ν_{as}$ C-H	-CH$_3$
2967	2978	2978	2978	2978	$ν_s$ C-H	-CH$_3$
---	3444	3423	3423	3423	OH and SiOH	H-O-H and ≡Si-OH

Table C.3 - Characteristic frequency vibrations and respective structural units for the MTMS-derived aerogels with SDS and without surfactant.

Wavenumber (cm^{-1})			Vibration type	Structural unit
A	A_SDS_0.50	A_SDS_0.75		
421	421	411	δ O-Si-O	-O-Si-O-
549	538	549	v_s Si-O	SiO_2 defects
676	676	676	v_s Si-O-Si	$\equiv$Si-O-Si$\equiv$
782	771	782	v_s Si-O	$\equiv$Si-O-Si$\equiv$
856	856	856	v Si-C	Si-R
920	920	920	v_β Si-O	$\equiv$Si-OH
1026	1026	1026	v_{as} Si-O-Si	$\equiv$Si-O-Si$\equiv$
1121	1121	1121		
1270	1270	1270	δ_s C-H	Si-R
1387	1387	1408	δ_{as} C-H	Si-R
1609	1620	1620	δ H-O-H	H-O-H
---	---	---	v_s C=O	H_2C-CO-CH$_2$
2850	2840	2840	v_s C-H	-CH$_3$
2914	2914	2914	v_{as} C-H	-CH$_3$
2978	2978	2978	v_s C-H	-CH$_3$
3434	3434	3423	OH and SiOH	H-O-H and $\equiv$Si-OH

Appendix D – Mass percentages estimates of Si, C, H, O in the aerogels

- Theoretical mass percentages calculations

1st Scenario: Complete condensation

Repetition unit
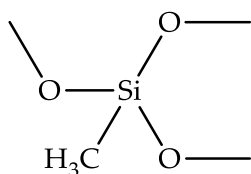
Molar ratios: 1 Si : 1 C : 3 H : 1.5 O

Through the calculated values, it is possible to evaluate the theoretical mass percentages knowing the molar mass of each element.

$$
\begin{aligned}
\text{Si} &= 28.09 \text{ g.mol}^{-1}\\
\text{C} &= 12.01 \text{ g.mol}^{-1}\\
\text{H} &= 1.00 \text{ g.mol}^{-1}\\
\text{O} &= 15.99 \text{ g.mol}^{-1}
\end{aligned}
$$

Thus,

$$\text{wt} = 1 \times 28.09 + 1 \times 12.01 + 3 \times 1.00 + 1.5 \times 15.99 = 67.085 \text{ g}$$

In order to know the mass percentage of each element, it follows:

$$\% \text{ C} = \frac{\text{number of atoms}_{\text{element}} \times M_{\text{element}}}{\text{wt}} \times 100 = \frac{1 \times 12.01}{67.085} \times 100 = 17.9\%$$
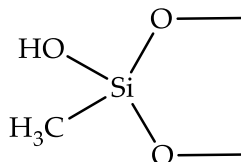
$$\% \text{ H} = \frac{3 \times 1.00}{67.085} \times 100 = 4.5\%$$

$$\% \text{ Si} + \% \text{O} = 100\% - \%\text{C} - \%\text{H} = 77.6\%$$

Base mass percentages: 17.9 C : 4.5 H : 77.6 Si+O

2nd Scenario: Incomplete condensation

Repetition unit

Molar ratios: 1 Si : 1 C : 3 H : 2 O

Through the calculated values, it is possible to evaluate the theoretical mass percentages knowing the molar mass of each element.

$$
\begin{aligned}
\text{Si} &= 28.09 \text{ g.mol}^{-1} \\
\text{C} &= 12.01 \text{ g.mol}^{-1} \\
\text{H} &= 1.00 \text{ g.mol}^{-1} \\
\text{O} &= 15.99 \text{ g.mol}^{-1}
\end{aligned}
$$

Thus,

$$\text{wt} = 1 \times 28.09 + 1 \times 12.01 + 3 \times 1.00 + 2 \times 15.99 = 76.08 \text{ g}$$

In order to know the mass percentage of each element, it follows:

$$\% \text{ C} = \frac{\text{number of atoms}_{\text{element}} \times M_{\text{element}}}{\text{wt}} \times 100 = \frac{1 \times 12.01}{76.08} \times 100 = 15.8\%$$

$$\% \text{ H} = \frac{3 \times 1.00}{76.08} \times 100 = 5.3\%$$

$$\% \text{ Si} + \%\text{O} = 100\% - \%\text{C} - \%\text{H} = 78.9\%$$

Base mass percentages: 15.8 C : 5.3 H : 78.9 Si+O

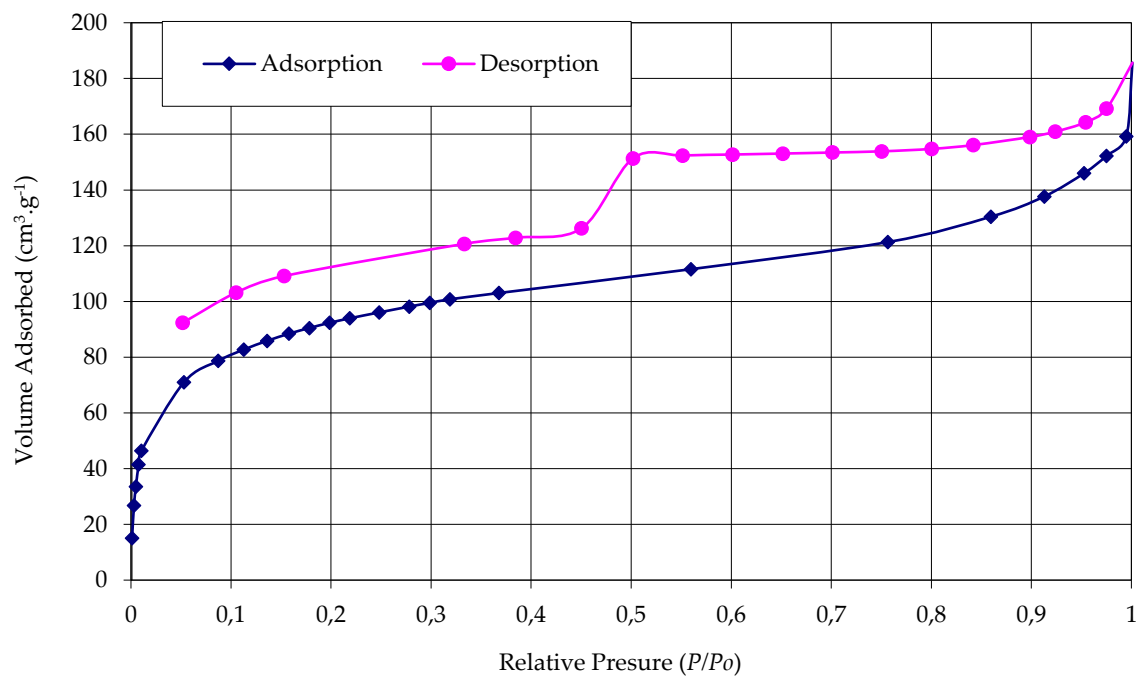# Appendix E – Adsorption-desorption isotherms

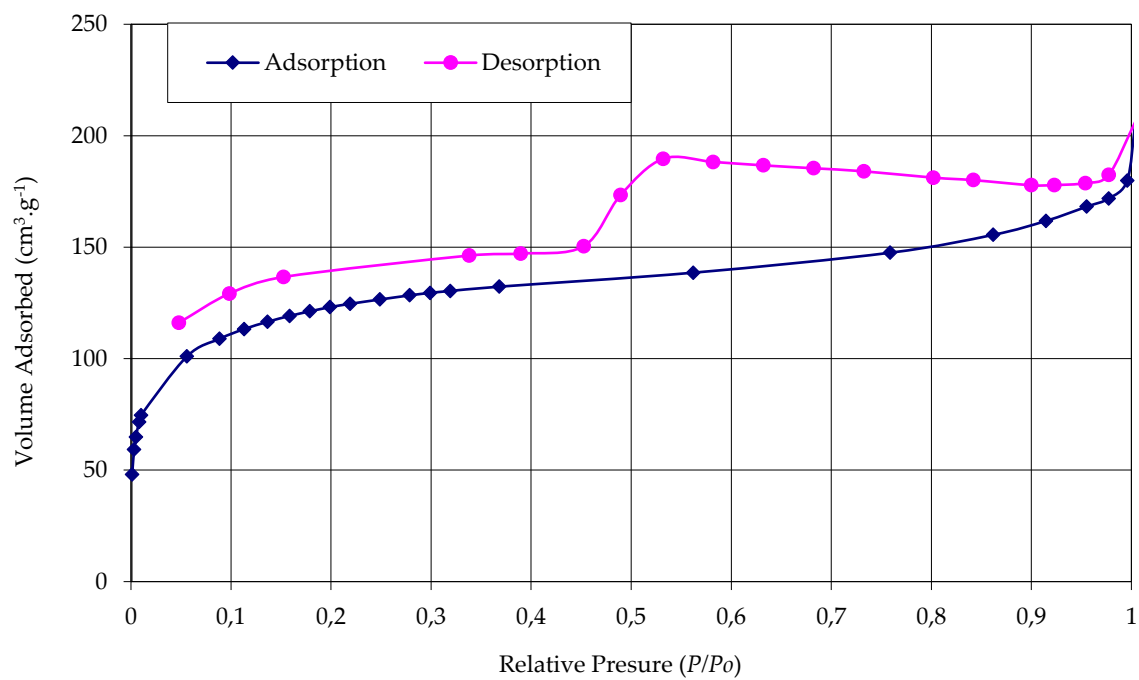Figure E.1 - Adsorption-desorption isotherms for sample A.

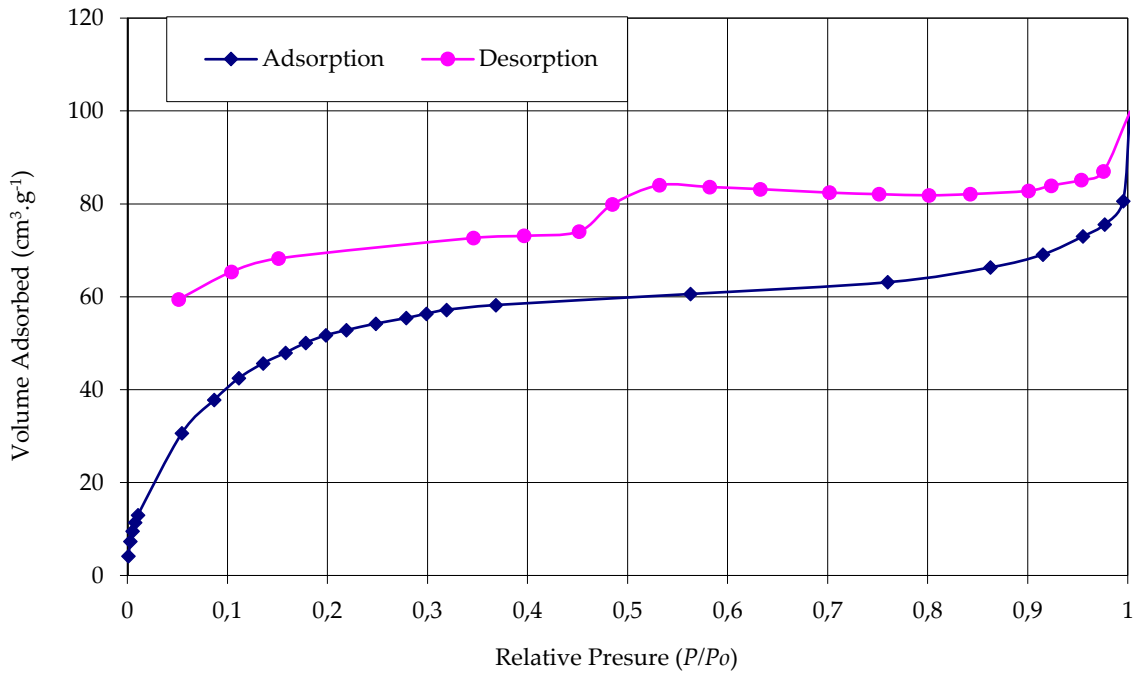Figure E.2 - Adsorption-desorption isotherms for sample A_CTAB_1.25.

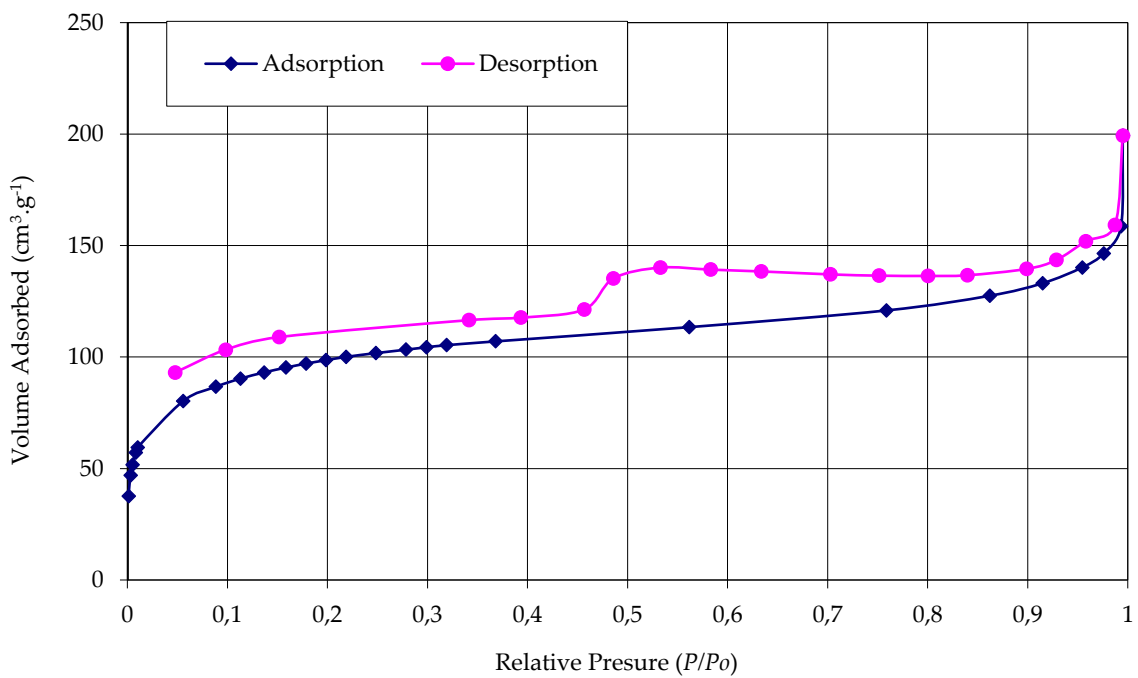Figure E.3 - Adsorption-desorption isotherms for sample A_F127_1.25.

Figure E.4 - Adsorption-desorption isotherms for sample A_SDS_0.75.

Appendix F – Simulation videos

Insert the CD to view the videos of the simulations.